Article

Novel Triazole-Piperazine Hybrid Molecules Induce Apoptosis via Activation of the Mitochondrial Pathway and Exhibit Anti-tumor Efficacy in Osteosarcoma Xenograft Nude Mice Model

Chandra Bhushan Mishra, Raj Kumar Mongre, Shikha Kumari, Dong Kee Jeong, and Manisha Tiwari

ACS Chem. Biol., **Just Accepted Manuscript** • DOI: 10.1021/acschembio.6b01007 • Publication Date (Web): 13 Jan 2017

Novel Triazole-Piperazine Hybrid Molecules Induce Apoptosis via Activation of the Mitochondrial Pathway and Exhibit Antitumor Efficacy in Osteosarcoma Xenograft Nude Mice Model

Chandra Bhushan Mishra[‡1], Raj Kumar Mongre[‡2], Shikha Kumari[‡1], Dong Kee Jeong[2]*, Manisha Tiwari[2]*

[1]Bio-organic Chemistry Laboratory, Dr. B.R. Ambedkar Center for Biomedical Research, University of Delhi, Delhi 110007, India

[2]Laboratory of Animal Genetic Engineering and Stem Cell Biology, Department of Animal Biotechnology and Advance Next Generation Convergence, Faculty of Biotechnology, Jeju National University, Jeju-Do, Republic of Korea

*Correspondence

Dr. Manisha Tiwari

Dr. B. R. Ambedkar Center for Biomedical

Research, University of Delhi, Delhi 110007, India

E-mail: mtiwari07@gmail.com

Professor Dong Kee Jeong

Department of Animal Biotechnology and Advance Next Generation Convergence,

Faculty of Biotechnology, Jeju National University, Ara-1 Dong, Jeju-city, Jeju-Do 690-756,

Republic of Korea

E-mail: dkjeong@jejunu.ac.kr

[‡]These authors have equal contribution.

Abstract

Mitochondria imparts crucial role in the regulation of programmed cell death, reactive oxygen species (ROS) generation besides serving as a primary energy source. Mitochondria appeared as an important target for therapy of cancer due to its significant contribution in cell survival and death. Here, we report the design and synthesis of a novel series of triazole-piperazine hybrids as potent anticancer agents. MCS-5 emerged as an excellent anticancer agent which showed better anticancer activity than standard drug Doxorubicin *in-vitro* and *in-vivo* studies. MCS5 displayed an IC_{50} value of 1.92 μM and induced apoptosis in Cal72 (human osteosarcoma cell line) cells by targeting mitochondrial pathway. This compound arrested G2/M phase of cell cycle, induced ROS production and mitochondrial potential collapse in Cal72 cells. MCS-5 displayed excellent anticancer activity in Cal72 Xenograft nude mice model where, it significantly reduced tumor progression leading to enhanced life span in treated animals compared to control and Doxorubicin treated animals without exerting noticeable toxicity. In addition, 2DG optical probe guided study clearly evokes that MCS-5 remarkably reduced tumor metastasis in Cal72 Xenograft nude mice model. These results indicate that MCS-5 appeared as a novel chemical entity which is endowed with excellent *in-vitro* as well as *in-vivo* anticancer activity and may contribute significantly for the management of cancer in the future.

Introduction

Cancer is a foremost reason of death worldwide and exerts a major health problem globally. 8.2 million deaths due to cancer in 2012 have been reported, which represents 13% of all deaths and 12.7 million new cases per year are being stated worldwide.[1] Cancer is a result of uncontrolled growth of abnormal cells and characterized by multiple structural, molecular and behavioral features. Out of all cancers types, liver, lung, bone, stomach, colon and breast cancer are

predominantly responsible for cancer mortality.[2] Treatment of cancer relies heavily on conventional therapies such as chemotherapy, radiotherapy, surgical removal as well as immunotherapy.[3-4]Since long time, widespread efforts have been done to counteract malignancies and in result various anticancer agents have been discovered.[5-8] However, clinically running anticancer drugs exert dreadful side effects, including cytotoxicity against normal cells.[9-10]

Osteosarcomas, the utmost communal malignancy of bone which affects 900 people per year in the United States.[11] It represents 56% of malignant bone tumors in children and nearby 3.4% of all childhood malignancies.[12] Currently, most effective chemotherapeutic agents for the treatment of osteosarcoma are Cisplatin, Doxorubicin and Methotrexate.[13] In spite of this, numerous new biological approaches to overcome osteosarcoma are being investigated which appear as fruitful strategies to prevent osteosarcoma and its metastasis.[14-16] Although several improvements in the management of osteosarcoma to date, quiet seems as a challenge because the overall survival rate of osteosarcoma patients has remained constant for over two decades therefore, new treatment approaches are necessarily required.

The mitochondria is the most important organelle concerned with the cellular bioenergetic and biosynthetic changes associated with cancer.[17-18] Mitochondrial alterations contribute to the invasive and metastatic properties in most of typical tumors. Therefore, the mitochondria is considered as a valuable target to induce apoptosis in cancer cells and numerous anticancer drugs follows the mitochondrial pathway to kill cancer cells.[19-20] The molecular hybridization of biologically active molecules is a powerful tool for drug discovery and appeared as a novel strategy to identify potential drug molecules against various diseases, including cancer.[21] Hybrid drug molecules may serve as a combination therapy in single multifunctional agent, which would

be more potent than conventional treatment approach.[22] Therefore, by adopting a molecule hybridization drug discovery approach, we aimed to design triazole-piperazine hybrid molecules as potent anticancer agents.

1,2,4-triazole is an important class of heterocycle which has been widely used to develop a large variety of bioactive molecules such as anti-bacterial, anti-fungal, anti-depressant, anti-oxidant, anti-inflammatory, anti-HIV and anti-tubercular agents.[23-26] 1,2,4-triazoles have also a successful history for the development of potent anticancer agent.[27-29] Various derivatives of 1,2,4-triazole derivatives were synthesized and tested for their anticancer potential in various *in-vitro* as well as *in-vivo* models (Fig. 1). For example, 4-amino-5-(5-phenylthiene-2-yl)-2,4-dihydro-3H-1,2,4-triazole-3-thione [30] (**1**) displayed excellent cytotoxicity against thymocytes with an IC_{50} value of 0.012 μM and 4-amino-5-mercapto-3-(2-chlorophenyl)-1,2,4-triazole [31] (**2**) displayed admirable antiproliferative activity in Ehrlich Ascites Carcinoma mice. Romagnoli et al. also synthesized a series of 1,5-disubstituted 1,2,4-triazole as potent anticancer agents.[32] Compound **3** showed excellent cytotoxicity against HeLa as well as Jurkat cells by inducing apoptosis.

On the other hand the piperazine moiety has also been used constantly to develop various potent anticancer agents and several piperazine containing molecules have shown admirable anticancer activities in both pre-clinical and clinical trials (Fig. 1).[33-34] The successful anticancer drug Imatinib [35] (**4)** also contains piperazine moiety and this drug is widely used to treat various types of cancer including chronic myelogenous leukemia. Additionally, a novel piperazine derivative **5** also (LYG-202) displayed potent anti-cancer activity *in vitro* and *in vivo* by inducing apoptosis.[36]

In continuation of our anticancer drug development agenda[37-39] and enthused by diverse anticancer properties of the triazole and piperazine moieties, we have designed a novel series of

triazole-piperazine hybrid molecules to appraise their *in-vitro* and *in-vivo* anticancer activity. This molecular hybridization might generate potential anticancer agent because both moieties (triazole and piperazine) are well studied to produce anticancer activity. Synthesized derivatives have been evaluated for their anti-proliferative activity against six types of cancer cell lines and their structure activity relationship has been also studied. The most active novel derivative MCS-5 showed remarkable cytotoxicity against Cal72 (human osteosarcoma cell line) without displaying cytotoxicity in normal cells. Therefore, MCS-5 was selected for further studies concerning its mechanism of action which governs apoptosis in Cal72 cells. Our studies have shown that MCS-5 activate the mitochondrial pathway to induce apoptosis process. MCS-5 has also exhibited noteworthy *in-vivo* antitumor activity in a xenograft mice model of human osteosarcoma. Additionally, this novel compound successfully reduced tumor metastasis in 2DG optical probe guided osteosarcoma-xenograft nude mice model. Our efforts have provided a novel chemical entity (MCS-5) with commendable anticancer activity which may help in the management of osteosarcoma in the future.

RESULTS AND DISCUSSION

Synthesis of triazole-piperazine hybrids. Designed novel hybrid molecules (**5-16**) have been synthesized in four steps which are depicted in scheme 1 (Fig. 2). In short, commercially available benzhydrazide **1** was reacted with carbon disulfide (CS_2) under reflux condition in dimethylformamide (DMF) to afford oxadiazole intermediate **2**. After that, compound **2** was reflux with hydrazine hydrate in 1,4-dioxane to yield aminotriazole intermediate **3**. Next, the amino group of aminotriazole (**3**) was reacted with furan-2- carboxyaldehyde in glacial acetic acid under reflux conditions, which led to the formation of furoyl-triazole derivative **4** in high yield. Finally, substituted piperazines were attached to triazole ring with a methylene linker by

performing the Mannich reaction providing the Mannich bases **5-16**. Synthesized compounds were fully characterized by ^{1}HNMR, ^{13}C NMR, Mass spectroscopy and elemental analysis.

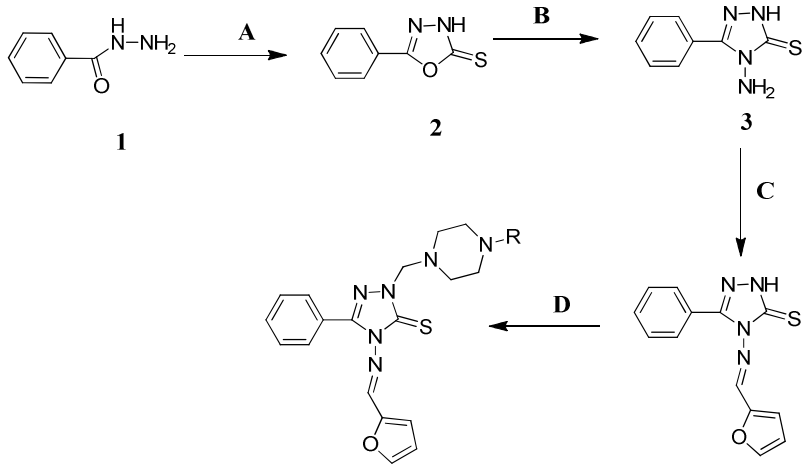

Compound Number	R-Group	Compound Number	R-Group
5	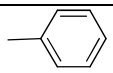	**11**	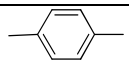
6	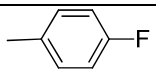	**12**	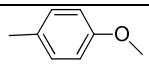
7	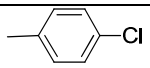	**13**	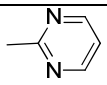
8	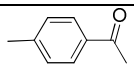	**14**	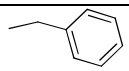
9	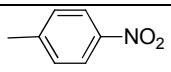	**15**	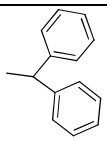

10	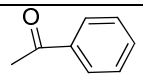	**16**	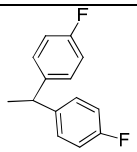

Scheme 1: Reagents and conditions: A. CS_2, DMF, reflux, 3-4 h; B. NH_2NH_2, 1,4 dioxane, reflux, 12-14 h; C. Furan-2- carboxyaldehyde, AcOH, reflux, 12-14 h; D. Substituted piperazine, formaldehyde, MeOH (reflux, 12-14 h)/ DMF(RT, 12-15 h).

***In-vitro* cytotoxicity studies and structure activity relationship (SAR)**: *In-vitro* cytotoxic potential of synthesized hybrids **5-16** were assessed against six types of human cancer cell lines; Cal72, HepG-2, SaOS-2, A549, MCF-7 and Hela by using MTT assay. The results are presented in terms of IC_{50} values as given in table 1. The structure activity relationship (SAR) has been explicated on the basis of observed results in MTT assay. It was observed that phenyl substitution (compound **5**) of this core was completely ineffective against all six cell lines. In electronegative element substituted phenyl derivatives, chloro substituted phenyl derivative (compound **7**) appeared more effective as compared to fluoro substituted derivative (compound **6)**. The chlorophenyl substituted derivative (compound **7**) was effective in producing cytotoxicity against Cal72 and MCF cell line even as fluorophenyl substituted derivative only showed satisfactory cytotoxicity towards the Hela cell line as compared to Doxorubicin. Ethanone group substitution on the phenyl ring (compound **8**) also did not exert satisfactory cytotoxicity against tested cell lines. However, this compound showed acceptable cytotoxicity against SaOS-2 cell line with an IC_{50} value of 15.76 μM which was almost similar to Doxorubicin. The introduction of NO_2 (strong electron withdrawing group) on the phenyl ring (compound **9**) displayed venerable cytotoxicity against the Cal72 cell line, while it did not show promising cytotoxicity towards other cell lines as compared to Doxorubicin. Benzoyl group

substitution (compound **10**, MCS-5) on this core made it a successful derivative and this compound showed excellent cytotoxicity against all tested six cancer cell lines. This compound displayed prominent cytotoxicity against Cal72, HepG-2, SaoS-2, MCF-7 as well as Hela cell line, where this compound showed much better IC_{50} value as compared to standard drug Doxorubicin. Electron donor methyl substitution on the phenyl ring (compound **11**) was unable to produce significant cytotoxicity against all tested six cancer cell lines. However, methoxy substituted phenyl derivative (compound **12**) exhibited promising cytotoxicity towards MCF-7 and Hela cell line as compared to Doxorubicin. Pyrimidine containing derivative (compound **13**) also did not produce a satisfactory cytotoxic effect against tested cancer cell lines. However, flexible benzyl moiety bearing derivative **14** showed promising cytotoxic effect against Cal72, HepG-2, SaOS-2 and Hela cell line as compared to Doxorubicin. The insertion of one more phenyl ring to the benzyl derivative led to diphenyl derivative **15** which showed significant cytotoxicity towards Cal72, SaoS-2, MCF-7 and Hela cell lines, where its efficacy was almost similar to Doxorubicin. Fluoro substitution at *p*-position of the diphenyl ring (compound **16**) also produced a remarkable cytotoxic effect against Cal72, HepG-2, MCF-7 and Hela cell line, where it appeared more potent than Doxorubicin.

In-vitro cytotoxicity of synthesized derivatives revealed that most of the compounds displayed a notable anticancer effect against tested cancer cell lines. Phase contrast microscopy images have been taken to elucidate morphological changes associated with programmed cell death (Fig. 2a). However, MCS-5 emerged as a most effective derivative in whole series and it showed admirable cytotoxicity against Cal72 with an IC_{50} value 1.97 μM in comparison with standard drug Doxorubicin which possesses an IC_{50} value 16.43 μM (Fig. 2b). Moreover, MCS-5 did not show significant cytotoxicity against normal human bone marrow (hBM) cell line and it also

demonstrated comparatively higher cell viability than Doxorubicin after 24 hours incubation (Fig. 2c). Additionally, time course studies of MCS-5 have been also performed against Cal72 cell line where, it gradually reduced cell viability up to 48 hours (Fig. 2d). Inspired with these results, we have chosen MCS-5 to proceed further for advance anticancer studies to confirm its potency as effective anticancer agent.

Table 1: *In-vitro* cytotoxic effect of novel synthesized compounds (**5-16**) [a]

Test compound	**IC_{50} (μM)[b]**					
	Cal72	**HepG-2**	**SaOS-2**	**A549**	**MCF-7**	**Hela**
5	44.73 ± 1.902	38.64 ± 0.816	32.31± 5.908	27.623± 2.109	23.20± 1.225	41.07± 3.645
6	17.20± 0.130	19.95± 0.022	39.32± 0.725	22.36± 1.556	42.13± 1.902	13.25± 0.380
7	16.04± 0.227	56.23± 0.492	51.87± 0.537	32.15± 0.529	19.25± 0.596	32.78± 0.759
8	18.75± 0.183	52.25± 0.435	15.76± 0.115	25.468± 0.602	34.28± 0.378	38.25± 0.642
9	3.93± 0.169	19.95± 0.663	16.65± 0.733	30.29± 0.943	35.39± 0.482	22.64± 0.466

10 (MCS-5)	1.97 ± 0.090	7.64± 0.509	9.99± 0.681	13.58± 0.779	6.34± 0.465	10.24± 0.442
11	27.31± 0.160	23.56± 0.345	19.02± 0.350	16.52± 0.328	26.81± 0.623	27.51± 0.104
12	18.14± 0.252	81.86± 36.234	19.91± 0.405	13.42± 0.170	10.21± 0.520	11.26± 1.234
13	22.52± 0.240	75.80± 0.600	39.94± 0.723	40.25± 1.418	52.36± 0.378	29.37± 0.352
14	16.18± 0.334	9.784± 0.285	8.678± 0.372	12.54± 0.755	16.25± 0.111	12.52± 0.200
15	16.39± 0.352	19.65± 0.226	15.07± 0.755	21.45± 1.211	14.27± 1.139	15.67± 0.236
16	4.702± 0.432	10.75± 0.837	24.78± 0.959	18.39± 0.459	12.73± 1.100	9.43± 0.429
Doxorubicin[c]	16.43± 0.352	17.31± 0.136	15.23± 0.220	8.27± 0.164	21.90± 0.432	14.52± 0.654

[a]The data denoted the mean of three experiments in triplicate and were value represented as mean.

[b] The IC_{50} denotes the concentration at which 50% of cells survived.

[C] Used as positive control

MCS-5 induces cell apoptosis. The generation of apoptosis has been regarded as a praiseworthy strategy for therapy of cancer and nearly all anticancer drugs kill tumor cells by inducing apoptotic processes.[40-41] Therefore, apoptotic effect of MCS-5 was assessed by Hoechst 33342 staining and propidium iodide (PI)/Annexin-V FITC double staining method in Cal72 cells. Phase contrast microscopy images have been taken to elucidate morphological alterations in the apoptotic cells by both staining methods as shown in Fig 3a. In Hoechst 33342 staining, MCS-5 treated cells showed distinctive apoptotic characteristics, including chromatin condensation, apoptotic body and nuclear fragmentation as compared to control and Doxorubicin (10 μM). Whereas, untreated cells displayed uniformly dispersed chromatin and stained meager homogeneous blue. Further, apoptosis induced by MCS-5 was also examined by microscopic study and flow cytometer using PI/Annexin-V FITC double staining method. Phase contrast microscopy of PI/Annexin-V FITC double staining MCS-5 treated cells displayed significant early and late apoptosis as compared to untreated cells (Fig. 3b). Flow cytometry studies markedly indicate that MCS-5 showed superior apoptosis against Cal72 cells as compared to Doxorubicin (Fig. 3c). The result of this study indicates that MCS-5 showed significant (P<0.05) apoptosis against Cal72 cells at both concentrations (5 μM and 10 μM). MCS-5 showed 14.82% and 31.40% apoptosis at 5 μM and 10 μM concentration, respectively, while Doxorubicin displayed only 7.00% apoptosis (Fig. 3c, 3d).

Effect of MCS-5 on Cell cycle arresting. Spontaneous cell divisions of cancer cells occur due to dysregulation of cell cycle, therefore inhibition of the cell cycle plays an important role in treating proliferative disease like cancer.[42] Most of the anticancer drugs disturbs the proliferation cycle of cancer cells by blocking cell cycle events which activate apoptosis.[43] Cell cycle arresting

potential of MCS-5 was assessed in Cal72 cells by a flow cytometric analysis. Results showed that MCS-5 effectively arrested the cell cycle in G2/M phase (Fig. 2e, 2f) and it has significantly raised Cal72 cell population in G2/M phase as compared to untreated cells. Upon MCS-5 treatment, the percentage of cells in G2/M phase were 25.47% and 21.65% at 5 and 10 μM, respectively, while, untreated cells displayed 10.79% cells in G2/M phase.

MCS-5 activates intrinsic apoptotic pathway: In order to explore the detailed mechanism of action of MCS-5 which directs apoptosis in Cal72, various associated pro-apoptotic and anti-apoptotic protein expression levels were checked by immunocytochemistry (ICC), mRNA quantification as well as immunoblotting assay. Bcl-2 act as a suppressor of apoptosis by blocking migration of cytochrome c, while pro-apoptotic members such as Bax work as promoters of apoptosis.[44] Our results revealed that MCS-5 treatment significantly (P<0.05) reduced anti-apoptotic protein Bcl-2 and increased pro-apoptotic Bax protein at transcriptional as well as translational level (Fig. 4a-g). In qualitative ICC analysis, down regulation of Bcl-2 and up-regulation of Bax was also noticed (Fig.4c). Next, we intended to analyze migration of cytochrome c from mitochondria to cytosol, which is a hallmark marker of apoptosis mediated through intrinsic pathway. q-PCR, Immunofluorescence, and Immunoblot studies revealed that treatment of MCS-5 markedly decreases mitochondrial cytochrome c that led to increased levels of cytochrome c in cytosol. (Fig. 4h-k). Cytochrome c binds with apoptotic activator factor-1(APAF-1) and thereby, forming apoptosome which activates caspase-9 followed by activation of caspase-3 leading to precede apoptosis through intrinsic pathway.[45] Therefore, we made an attempt to explicate the effect of MCS-5 on APAF-1, caspase-3 and caspase-9 regulation by ICC, qPCR and western blot analysis. Interestingly, our findings clearly demonstrated that treatment of MCS-5 significantly (P<0.05) up regulate APAF-1, caspase-9 and capase-3 at both

transcriptional and translational level, which further confirmed their involvement in the intrinsic pathway to induce apoptosis by formation of apoptosome complex (Fig. 5a-5i). These proteins up regulation have been also visualized in ICC studies where strong fluorescence intensity was seen in MCS-5 treated cells as compared to untreated cells (Fig.5c, 5g). After that, we have inspected impact of MCS-5 on p53 activation; p53 is the most extensively studied tumor suppressor which mediates apoptosis primarily through the intrinsic apoptotic pathway and may also trans-activate numerous components of the apoptotic effectors machinery.[46] Consequently, our results showed that after 24 hours treatment MCS-5 remarkably increased p53 expression in Cal72 cells as compared to untreated cells, which was quantified by qPCR analysis and also captured in immunofluorescence staining (Fig. 6a, 6b). Over expression of p53 was also appeared in western blot analysis as compared to untreated cells and Doxorubicin treated cells (Fig. 6c, 6d). p53 activation is escorted by down regulation of c-MYC expression and both are considered as a decisive factor of cell to undergo apoptosis.[47] Thus, activation of p53 by MCS-5 stimulated apoptotic effectors machinery, which led to induce apoptosis via intrinsic pathway. Overall, all these studies evidently supports, triggering of the intrinsic pathway of apoptosis by MCS-5 which directs apoptosis in Cal72 cells.

MCS-5 down regulates NF-κB and IL-6 level. Suppression of NF-κB activity plays important role in stimulation of apoptotic process and it is a key decisive factor in the selection of drugs for therapy of cancer.[48] Moreover, interleukin-6 (IL-6) is an attractive target for cancer therapy and its inhibition encourages apoptosis progression in cancer cells. IL-6 is regulated by the transcription factor NF-κB and built a significant link between inflammation initiation and progression of angiogenesis.[49] ICC studies visibly pointed out the down regulation of NF-κB and IL-6 after MCS-5 treatment (Fig. 6j, 6k). Addition to this, MCS-5 treatment significantly

reduced m-RNA level of NF-κB and IL-6 as compared to untreated and Doxorubicin treated cells (Fig. 6e, 6f). Furthermore, western blot analysis also certified reduction of NF-κB and IL-6 at the proteomic level in MCS-5 treated cells as compared to untreated cells (Fig. 6g-i). Thus, our results indicate that MCS-5 impressively down regulates NF-κB and IL-6 resulting to collapse mitochondrial integrity and initiate apoptosis in Cal72 cells.

MCS-5 induce ROS level enhancement in Cal72 cells: Reactive oxygen species (ROS) are generated as by-products of respiration and their levels are very high during cell apoptosis.[50] Mitochondria is the major creator of ROS in mammalian cells, and its dysfunction increases high ROS levels, which led to induce cell apoptosis process.[51] Hence, we assessed intercellular ROS levels using DCFDA dye by FACS and phase contrast microscopy. FACS analysis showed that MCS-5 increases ROS levels in a concentration dependent manner where, it showed 38 %, 58 % and 62 % ROS induced cells at 5, 10 and 15 μM concentration, respectively (Fig. 7c, 7d). Enhanced fluorescence intensity after treatment of MCS-5 as compared to untreated cells in phase contrast microscopy further validate ROS inducing capability of MCS-5 (Fig. 7e). Both studies noticeably indicate that MCS-5 induced ROS production in Cal72 cells, which impart progression of cell apoptosis through the mitochondria.

MCS-5 induces depolarization and loss of mitochondrial transmembrane potential ($\Delta\Psi m$). A decrease of mitochondrial transmembrane potential ($\Delta\Psi m$) is well acknowledged during an early event of apoptosis and considered as a hallmark of cells, which proceeding apoptosis through mitochondrial insult.[52] We have measured loss of $\Delta\Psi m$ in MCS-5 treated Cal72 cells using JC-1 staining by flow cytometer and $\Delta\Psi m$ was also pictured by phase contrast microscopy. Microscopic results showed that MCS-5 induced strong green fluorescence and reduced red fluorescence as compared to untreated cells and Doxorubicin treated cells in Cal72 cells, which

suggests potential deduction of $\Delta\Psi m$ by this compound at both concentrations (5 μM and 10 μM) (Fig. 7b). Consequently, flow cytometry result also showed a loss of mitochondrial potential in MCS-5 treated cell as compared to untreated cell. At 5 μM and 10 μM concentrations it showed 18.17 % and 34.67 % cell population, which emit green fluorescence, respectively, while untreated cells displayed 1.97 % green fluorescence emitting cells (Fig 7a). In this study Doxorubicin at 5 μM and 10 μM have been shown 14.83 % and 12.56 % cell population, respectively which produce green fluorescence. Hence, MCS-5 strongly induced mitochondrial potential deficit in Cal72 cells as compared to Doxorubicin (Fig. 7a, b). These studies suggest that MCS-5 significantly induced mitochondrial potential collapse in Cal72 cells, which lead to activate cell apoptosis.

MCS-5 exhibits tumoricidal effects in Cal72 xenograft nude mice model. The *in-vivo* anticancer action of MCS-5 was judged in osteosarcoma xenograft animal model using immunodeficient nude mouse at the dose of 5 and 10 mg/kg body weight (bwt). A successfully developed model was treated with both doses for 45 days and Doxorubicin (10 mg/kg, bwt) was used as a positive control. Firstly, routine investigation of MCS-5 efficacy on survivability of mice has been analyzed by Log-rank test. The Kaplan-Meier curves demonstrate that orthotopic tumor-bearing mice treated with MCS-5 at 10 mg/kg/day exhibited significantly enhanced survival rate than 5 mg/kg/day MCS-5 or 10 mg/kg/day Doxorubicin or vehicle-treated controls (Fig. 8a, b). The results point out that MCS-5 increased almost double life span (survival rate= 63 %) of animals as compared to untreated animals (survival rate= 32 %). Additionally, MCS-5 at the dose 10 mg/kg significantly increased life span of tumor bearing mice 32 to 62 % compared to Doxorubicin (32 to 52 %). Furthermore, MCS-5 (10 mg/kg/day) significantly attenuated tumor size as compared to control animals (Fig. 8c). To validate our studies, tumors

were removed and weighed and it was witnessed that MCS-5 (10 mg/kg) significantly (P<0.01) reduced tumor weight as compared to Doxorubicin (Fig. 8d). Also, MCS-5 (10 mg/kg) significantly reduced tumor volume over time as compared to untreated and Doxorubicin (10mg/kg) treated animals (Fig. 8e). These results clearly evoke the efficacy of MCS-5 to conquer Cal72 induced osteosarcoma nude mice model.

MCS-5 inhibits tumor metastasis in Cal72 xenograft nude mice model. To evaluate whether the robust anti-neoplastic efficacy of MCS-5 observed *in-vivo* live tumor resection and dissemination, we established optical probe guided tumor imaging model. Infra-red (IR) dye-800CW-2-deoxy-D-glucose (2DG) wavelength-based whole body images were captured to visualize the effect of MCS-5 to slow down tumor metastases in MCS-5 treated animals (Fig. 9a-c). 2DG is extensively used tracer to mark out tumor progression and metastases because the rate of glycolysis in tumor cells and metastasized body organs is significantly enhance.[53] 2DG optical probe guided fluorescence imaging studies displayed that MCS-5 at the dose of 10 mg/kg/day successfully stopped tumor metastasis in tumor bearing animals. Tumor metastasis was clearly visible in untreated tumor bearing animals while MCS-5 treated animals did not show any metastasized tumor. Thus, we can conclude that MCS-5 rewardingly abridged tumor and its metastasis in the osteosarcoma nude mice model.

Toxicity evaluation. Toxicity and side-effects of the MCS-5 were assessed by monitoring the relative body weight, behavioral appearance, intake of water and food of animals on a daily basis. Analysis showed that there was no statistically significant difference seen in body weight (assessed as a percentage of the initial body weight) between the MCS-5 treatment group and the control (normal mice) observed which suggests that MCS-5 treatment was not overtly toxic for

the mice. Moreover, no behavioral changes were observed, including any alteration in food and water intake during whole experimental period. Although, a significantly reduction the body weight was observed in Doxorubicin treated group (Fig. 9d).

Conclusion

In conclusion, synthesized novel triazole-piperazine hybrid molecules displayed moderate to excellent cytotoxicity against six cell lines. MCS-5 appeared as a most active derivative and it displayed better cytotoxicity as compared to Doxorubicin in Cal72 cells. This compound showed magnificent apoptotic potential in Cal72 cells and arrested cells in the G2/M phase of the cell cycle. Mechanistic studies revealed that MCS-5 activate the mitochondrial pathway to induce apoptosis in Cal72 cells where it up regulates/down regulates a number of proteins which are involved in mitochondrial associated intrinsic pathway of apoptosis. Further, MCS-5 excellently induced ROS generation and loss of $\Delta\Psi m$ in Cal72 cells. Furthermore, this derivative displayed remarkable tumoricidal effect in Cal72-xenograft nude mice model without producing significant toxicity in animals. In addition to this MCS-5 significantly stop tumor metastasis in the osteosarcoma nude mice model. Thus, investigation provided a potent anticancer agent MCS-5 which showed the excellent anticancer effect *in-vitro* and *in-vivo* models by triggering mitochondrial pathway of apoptosis.

METHODS

Chemistry. All the commercial starting material and organic solvents were procured from TCI Chemicals (Tokyo, Japan), Sigma Aldrich (St. Louis, MO, USA), Alfa Aesar (Massachusetts, U.S States), and Merck (Darmstadt, Germany). The solvents which were used for reaction medium were dried by standard methods. ^{1}H and ^{13}C nuclear magnetic resonance (NMR) spectra were acquired by high resolution Jeol NMR spectrophotometer (USA) at 400 and 100 MHz, respectively. Chemical shifts are reported in parts per million (ppm) relative to the solvent peak

or tetramethylsilane (TMS). The coupling constants (*J*) are reported in hertz (Hz) and the splitting patterns are described by using the following abbreviations: s, (singlet); d, (doublet); t, (triplet); m, (multiplet); brs, (broad singlet); dd, (double doublet). LC/MS data were recorded on Agilent 6310 Ion trap LC/MS system. Melting points were determined in open capillaries using model KSPII, KRUSS, (Germany) and elemental analysis (C, H and N) was carried on Elementar analysensysteme. Purity of the target compounds was determined by on a Shimadzu HPLC system (Kyoto, Japan) coupled with a photodiode array detector (PDA) and C-18 column. All final compounds reported here showed more than 95% HPLC purity

Procedure for the synthesis of 5-phenyl-1,3,4-oxadiazole-2(3H)-thione (2)

Benzoic hydrazide (1 Molar) and carbon disulphide (3 Molar) were reacted in dried DMF at room temperature (RT) for 20 minutes. Then after, the reaction mixture was heated at a reflux temperature for 3-4 hours. Upon completion, the reaction mixture was poured into ice-cold water to obtain white colored precipitate. The obtained product was washed twice with water and petroleum ether to yield pure compound **2**.

5-phenyl-1,3,4-oxadiazole-2(3H)-thione (2)

Yield: 95%; White solid; mp: 207-209˚C; ^{1}H NMR (DMSO-d_6, 400 MHz): δ 7.58-7.56 (m, 3H), 7.85-7.84 (m, 2H, Ar), 14.81 (brs, 1H, SH); LC-MS: m/z, 179 (M+1).

Procedure for the synthesis of 4-amino-3-phenyl-1H-1,2,4-triazole-5(4H)-thione (3)

A suspension of intermediate **2** (1 Molar) and hydrazine hydrate (50 Molar), in 1,4-dioxane was refluxed for 12-14 hours. The color of the reaction mixture was changed into green, with the evolution of hydrogen sulfide gas. After completion, the reaction mixture was cooled on ice and acidified with conc. hydrochloric acid. The product obtained was washed twice with tap water and then with petroleum ether to yield pure compound **3**.

4-amino-3-phenyl-1H-1,2,4-triazole-5(4H)-thione (3)

Yield: 88%; White solid; mp: 206-208˚C; ^{1}H NMR (DMSO-d_6, 400 MHz): δ 5.74 (s, 2H, NH_2), 7.49-7.47 (m, 3H, Ar), 7.96-7.94 (m, 2H, Ar), 13.89 (brs, 1H, SH); LC-MS: m/z, 193 (M+1).

Procedure for the synthesis of 4-((furan-2-ylmethylene)amino)-3-phenyl-1H-1,2,4-triazole-5(4H)-thione (4)

2-Furaldehyde and intermediate **3** were taken in equimolar ratio and refluxed for 12-14 hours. Upon reaction completion, the reaction mixture was poured into ice-cold water to crude product. The obtained product was filtered and washed with water thrice. Then after, it was crystallized from chloroform/methanol mixture to afford pure compound **4**.

4-((furan-2-ylmethylene)amino)-3-phenyl-1H-1,2,4-triazole-5(4H)-thione (4)

Yield: 74%; Creamish solid; mp: 182-184˚C; ^{1}H NMR (DMSO-d_6, 400 MHz): δ 6.78-6.76 (m, 1H, Ar), 7.37 (d, 1H, Ar, *J*=4.2 Hz), 7.52-7.50 (m, 3H, Ar), 7.86-7.81 (m, 2H, Ar), 8.06 (m, 1H, Ar), 9.54 (s, 1H, CH), 14.19 (s, 1H, SH); LC-MS: m/z, 271 (M+1).

General Procedure for the synthesis of 4-((furan-2-ylmethylene)amino)-3-phenyl-1-(substituted-piperazin-1-yl)methyl)-1H-1,2,4-triazole-5(4H)-thione

The equimolar molar ratio of substituted piperazine derivative and intermediate **4** was reacted either in methanol (anhydrous) under reflux condition for 12-14 hours or DMF at room temperature for 12-15 hours in the presence of formaldehyde (equimolar ratio). The reaction mixture was diluted with water to give precipitation of the desired compound. The crude products were filtered and purified by column chromatography using chloroform/methanol (97:03) as eluent.

4-((furan-2-ylmethylene)amino)-3-phenyl-1-((4-phenylpiperazin-1-yl)methyl)-1H-1,2,4-triazole-5(4H)-thione (5)

Yield: 69%; Creamish solid; mp: 68-70˚C; ^{1}H NMR (DMSO-d_6, 400 MHz): δ 2.89-2.93 (m, 4H, piperazine), 3.10-3.13 (m, 4H, piperazine), 5.24 (s, 2H, CH_2), 6.72-6.79 (m, 2H, Ar), 6.88 (d, 2H, Ar, *J*=8.2 Hz), 7.16 (t, 2H, Ar, *J*=8.2Hz), 7.39 (d, 1H, Ar, *J*=3.6Hz), 7.50-7.56 (m, 3H, Ar), 7.84-7.88 (m, 2H, Ar), 8.07 (s, 1H, Ar), 9.48 (s, 1H, CH); LC-MS: m/z, 444 (M+); Anal. Calcd for $C_{24}H_{24}N_6OS$: C, 64.84; H, 5.44; N, 18.90; Found: C, 64.59; H, 5.64; N, 19.11.

1-((4-(4-fluorophenyl)piperazin-1-yl)methyl)-4-((furan-2-ylmethylene)amino)-3-phenyl-1H-1,2,4-triazole-5(4H)-thione (6)

Yield:73%; White solid; mp: 75-77˚C; ^{1}H NMR (DMSO-d_6, 400 MHz): δ 2.92 (s, 4H, piperazine), 3.07 (s, 4H, piperazine), 5.23 (s, 2H, CH_2), 6.77-6.78 (m,1H, Ar), 6.90-6.92 (m, 2H, Ar), 7.00 (m, 2H, Ar), 7.38 (d, 1H, Ar, *J*=3.0 Hz), 7.75-7.54 (m, 3H, Ar), 7.86-7.88 (m, 2H, Ar), 8.06 (s, 1H, Ar), 9.51 (s, 1H, CH); ^{13}C NMR ($CDCl_3$, 100 MHz): δ 50.3, 50.4, 69.2, 112.5, 115.3, 115.5, 118.1, 118.9, 125.1, 128.5, 128.7, 130.7, 147.0, 147.7, 147.9, 148.1, 151.8, 156.0, 158.3, 163.6; LC-MS: m/z, 463 (M+1); Anal. Calcd for $C_{24}H_{23}FN_6OS$: C, 62.32; H, 5.01; N, 18.17; Found: C, 62.63; H, 5.28; N, 17.95.

1-((4-(4-chlorophenyl)piperazin-1-yl)methyl)-4-((furan-2-ylmethylene)amino)-3-phenyl-1H-1,2,4-triazole-5(4H)-thione (7)

Yield:88%; White solid; mp: 85-87˚C; ^{1}H NMR (DMSO-d_6, 400 MHz): δ 2.90 (s, 4H, piperazine), 3.13 (s, 4H, piperazine), 5.24 (s, 2H, CH_2), 6.78-6.80 (m, 1H, Ar), 6.91 (d, 2H, Ar, *J*=9.1 Hz),7.19 (d, 2H, Ar, *J*=8.5 Hz), 7.39 (d, 1H, Ar, *J*=3.6 Hz), 7.54-7.56 (m, 3H, Ar), 7.85-7.87 (m, 2H, Ar), 8.08 (s, 1H, Ar), 9.48 (s, 1H, CH); ^{13}C NMR (DMSO-d_6, 100 MHz): δ 48.1, 49.7, 68.9, 113.1, 117.0, 121.0, 122.3, 124.9, 125.0, 128.4, 128.6, 128.7, 130.9, 147.0, 147.4, 148.4, 149.8, 155.8, 163.1; LC-MS: m/z, 480 (M+1); Anal. Calcd for $C_{24}H_{23}ClN_6OS$: C, 60.18; H, 4.84; N, 17.55; Found: C, 60.37; H, 4.61; N, 17.82.

1-(4-(4-((4-((furan-2-ylmethylene)amino)-3-phenyl-5-thioxo-4,5-dihydro-1H-1,2,4-triazol-1-yl)methyl)piperazin-1-yl)phenyl)ethanone (8)

Yield:59%; White solid; mp: 105-107˚C; ^{1}H NMR (DMSO-d_6, 400 MHz): δ 2.41 (s, 3H, CH_3), 2.90 (s, 4H, piperazine), 3.35 (s, 4H, piperazine), 5.25 (s, 2H, CH_2), 6.77-6.79 (m, 1H, Ar), 6.94 (d, 2H, Ar, *J*=8.5 Hz), 7.37 (d, 1H, Ar, *J*=4.8 Hz), 7.51-7.56 (m, 3H, Ar), 7.76 (d, 2H, Ar, *J*=9.1 Hz), 7.84-7.87 (m, 2H, Ar), 8.07 (s, 1H, Ar), 9.47 (s, 1H, CH); ^{13}C NMR (DMSO-d_6, 100 MHz): δ 26.0, 46.6, 49.6, 68.9, 113.1, 121.1, 125.1, 126.7, 128.4, 128.8, 130.0, 130.9, 148.4, 153.6, 155.8, 163.3, 195.6; LC-MS: m/z, 487 (M+1); Anal. Calcd for $C_{26}H_{26}N_6O_2S$: C, 64.18; H, 5.39; N, 17.27; Found: C, 63.84; H, 5.23; N, 17.07.

4-((furan-2-ylmethylene)amino)-1-((4-(4-nitrophenyl)piperazin-1-yl)methyl)-3-phenyl-1H-1,2,4-triazole-5(4H)-thione (9)

Yield:73%; Pale yellow solid; mp: 151-153˚C; ^{1}H NMR (DMSO-d_6, 400 MHz): δ 2.86 (t, 4H, piperazine, *J*=5.4 Hz), 3.43 (t, 4H, piperazine, *J*=5.4Hz), 5.21 (s, 2H, CH_2), 6.75-6.72 (m, 1H, Ar), 6.94 (d, 2H, Ar, *J*=9.1Hz), 7.32 (d, 1H, Ar, *J*=4.2Hz), 7.52-7.45 (m, 3H, Ar), 7.81 (d, 2H, Ar, *J*=7.9Hz), 7.96 (d, 2H, Ar, *J*=9.2Hz), 8.02 (s, 1H, Ar), 9.44 (s, 1H, CH); ^{13}C NMR (DMSO-d_6, 100 MHz): δ 46.3, 49.5, 68.7, 112.6, 113.1, 120.8, 124.9, 125.7, 128.4, 128.7, 131.0, 136.8, 147.0, 147.3, 148.4, 154.6, 155.8, 163.1; LC-MS: m/z, 490 (M+1); Anal. Calcd for $C_{24}H_{23}N_7O_3S$: C, 58.88; H, 4.74; N, 20.03; Found: C, 59.16, H, 4.90; N, 19.71.

(4-((4-((furan-2-ylmethylene)amino)-3-phenyl-5-thioxo-4,5-dihydro-1H-1,2,4-triazol-1-yl)methyl)piperazin-1-yl)(phenyl)methanone (10)

Yield:78%; White solid; mp: 72-74˚C; ^{1}H NMR ($CDCl_3$, 400 MHz): δ 2.80-3.03 (m, 4H, piperazine), 3.34 (s, 2H, piperazine), 3.81 (s, 2H, piperazine), 5.28 (s, 2H, CH_2), 6.59-6.61 (m, 1H, Ar), 7.10 (d, 1H, Ar, *J*=3.8 Hz),7.34-7.39 (m, 5H, Ar), 7.45-7.49 (m, 3H, Ar), 7.68 (s, 1H, Ar), 7.95-8.01 (m, 2H, Ar), 9.99 (s, 1H, CH); ^{13}C NMR ($CDCl_3$, 100 MHz): δ 42.0, 47.6, 50.6, 69.2, 112.6, 119.0, 125.0, 127.0, 128.3, 128.5, 128.6, 129.6, 130.8, 135.4, 147.0, 147.7, 148.2, 151.9, 163.6, 170.3; LC-MS: m/z, 473 (M+1); Anal. Calcd for $C_{25}H_{24}N_6O_2S$: C, 63.54; H, 5.12; N, 17.78; Found: C, 63.27; H, 4.93; N; 18.04.

4-((furan-2-ylmethylene)amino)-3-phenyl-1-((4-(p-tolyl)piperazin-1-yl)methyl)-1H-1,2,4-triazole-5(4H)-thione (11)

Yield:83%; White solid; mp: 152-154˚C; ^{1}H NMR ($CDCl_3$, 400 MHz): δ 2.25 (s, 3H, CH_3), 3.04-3.06-3.15 (m, 8H, piperazine), 5.32 (s, 2H, CH_2), 6.59-6.60 (m, 1H, Ar), 6.82 (d, 2H, Ar, *J*=8.4 Hz), 7.04-7.10 (m, 3H, Ar), 7.45-7.50 (m, 3H, Ar), 7.67 (s, 1H, Ar), 7.96-7.98 (m, 2H, Ar), 10.01 (s, 1H, CH); ^{13}C NMR ($CDCl_3$, 100 MHz): δ 20.3, 49.9, 50.4, 69.3, 112.5, 116.7, 118.9, 125.2, 128.5, 128.7, 129.4, 129.5, 130.7, 147.0, 147.8, 148.1, 149.1, 151.8, 163.6; LC-MS: m/z, 459 (M+1); Anal. Calcd for $C_{25}H_{26}N_6OS$: C, 65.48; H, 5.71; N, 18.33; Found: C, 65.22; H, 5.88; N, 18.64.

4-((furan-2-ylmethylene)amino)-1-((4-(4-methoxyphenyl)piperazin-1-yl)methyl)-3-phenyl-1H-1,2,4-triazole-5(4H)-thione (12)

Yield:69%; Cream solid; mp: 160-162˚C; ^{1}H NMR ($CDCl_3$, 400 MHz): δ 3.08-3.09 (m, 8H, piperazine), 3.75 (s, 3H, CH_3), 5.31 (s, 2H, CH_2), 6.58-6.61(m, 1H, Ar), 6.81-6.89 (m, 4H, Ar), 7.09 (d, 1H, Ar, *J*=7.9Hz), 7.48-7.49 (m, 3H, Ar), 7.67 (m, 1H, Ar), 7.96-8.00 (m, 2H, Ar), 10.01 (s, 1H, CH); ^{13}C NMR ($CDCl_3$, 100 MHz): δ 29.6, 59.3, 62.4, 112.6, 119.2, 124.5, 124.7, 125.1, 128.0, 128.2, 128.5, 130.8, 146.9, 147.1, 147.6, 151.1, 152.0, 163.3; LC-MS: m/z, 475 (M+1); Anal. Calcd for $C_{25}H_{26}N_6O_2S$: C, 63.27; H, 5.52; N, 17.71; Found: C, 63.54; H, 5.75; N, 17.47.

4-((furan-2-ylmethylene)amino)-3-phenyl-1-((4-(pyrimidin-2-yl)piperazin-1-yl)methyl)-1H-1,2,4-triazole-5(4H)-thione (13)

Yield:83%; Creamish solid; mp: 128-130˚C; ^{1}H NMR ($CDCl_3$, 400 MHz): δ 2.96 (t, 4H, piperazine, *J*= 4.8 Hz), 3.87 (t, 4H, piperazine, *J*=5.1Hz), 5.31 (s, 2H, CH_2), 6.44 (t, 1H, Ar, *J*=4.5Hz), 6.60 (t, 1H, Ar, *J*= 1.8Hz), 7.07 (d, 1H, Ar, *J*=3.6Hz), 7.48-7.44 (m, 3H, Ar), 7.67 (s, 1H, Ar), 7.96-7.94 (m, 2H, Ar), 8.25 (d, 2H, Ar, *J*=4.8Hz), 10.0 (s, 1H, CH); ^{13}C NMR ($CDCl_3$, 100 MHz): δ 43.5, 50.4, 69.5, 109.7, 112.5, 118.9, 125.1, 128.5, 128.7, 130.7, 147.0, 147.8, 148.1, 151.7, 157.6, 161.4, 163.6; LC-MS: m/z, 447 (M+1); Anal. Calcd for $C_{22}H_{22}N_8OS$: C, 59.18; H, 4.97; N, 25.09; Found: C, 59.52; H, 5.12; N, 24.79.

1-((4-benzylpiperazin-1-yl)methyl)-4-((furan-2-ylmethylene)amino)-3-phenyl-1H-1,2,4-triazole-5(4H)-thione (14)

Yield:71%; Cream solid; mp: 60-62˚C; ^{1}H NMR (DMSO-d_6,400 MHz): δ 2.36 (s, 4H, piperazine), 2.77 (s, 4H, piperazine), 3.41 (s, 2H, CH_2), 5.16 (s, 2H, CH_2), 6.78-6.79 (m, 1H, Ar), 7.19-7.26 (m, 5H, Ar), 7.38 (d, 1H, Ar, *J*=3.6Hz), 7.51-7.54 (m, 3H, Ar), 7.84-7.89 (m, 2H, Ar), 8.08 (s, 1H, Ar), 9.49 (s, 1H, CH); ^{13}C NMR (DMSO-d_6, 100 MHz): δ 49.8, 52.3, 62.0, 70.9, 113.0, 120.3, 125.0, 126.9, 128.0, 128.4, 128.7, 130.9, 148.4, 155.4, 163.0; LC-MS: m/z, 459 (M+1); Anal. Calcd for $C_{25}H_{26}N_6OS$: C, 65.48; H, 5.71; N, 18.33; Found: C, 65.71; H, 5.50; N, 18.06.

1-((4-benzhydrylpiperazin-1-yl)methyl)-4-((furan-2-ylmethylene)amino)-3-phenyl-1H-1,2,4-triazole-5(4H)-thione (15)

Yield:89%; White solid; mp: 122-124˚C; ^{1}H NMR (DMSO-d_6, 400 MHz): δ 2.30 (s, 4H, piperazine), 2.80 (s, 4H, piperazine), 4.23 (s, 1H, CH), 5.15 (s, 2H, CH_2), 6.78-6.80 (m, 1H, Ar), 7.14 (t, 2H, Ar, *J*=8.8 Hz), 7.23 (t, 4H, Ar, *J*=7.6 Hz), 7.34-7.40 (m, 5H, Ar), 7.52-7.58 (m, 3H, Ar), 7.87-7.93 (m, 2H, Ar), 8.08 (s, 1H, Ar), 9.49 (s, 1H, CH); ^{13}C NMR (DMSO-d_6, 100 MHz): δ 49.9, 51.4, 69.0, 75.1, 113.1, 120.9, 125.0, 126.7, 127.4, 128.4, 128.7, 130.8, 142.8, 147.0, 147.2, 148.4, 155.7, 163.1; LC-MS: m/z, 535 (M+1); Anal. Calcd for $C_{31}H_{30}N_6OS$: C, 69.64; H, 5.66; N, 15.72; Found: C, 69.49; H, 5.48; N, 16.05.

1-((4-(bis(4-fluorophenyl)methyl)piperazin-1-yl)methyl)-4-((furan-2-ylmethylene)amino)-3-phenyl-1H-1,2,4-triazole-5(4H)-thione (16)

Yield:76%; Creamish solid; mp: 125-127˚C; ^{1}H NMR ($CDCl_3$, 400 MHz): δ 2.39 (s, 4H, piperazine), 2.90 (t, 4H, piperazine, *J*=4.5 Hz), 4.19 (s, 1H, CH), 5.24 (s, 2H, CH_2), 6.60-6.61 (m, 1H, Ar), 6.91-6.95 (m, 4H, Ar), 7.10 (d, 1H, Ar, *J*=3.0 Hz), 7.28-7.31 (m, 4H, Ar), 7.48-7.50 (m, 3H, Ar), 7.68 (d, 1H, Ar, *J*=1.8 Hz), 8.00-8.08 (m, 2H, Ar), 10.0 (s, 1H, CH); ^{13}C NMR (DMSO-d_6, 100 MHz): δ 50.0, 51.3, 69.0, 73.2, 113.2, 115.4, 121.1, 125.1, 128.6, 128.9, 129.4, 131.2, 138.8, 147.1, 147.4, 148.6, 156.0, 159.0, 163.3; LC-MS: m/z, 571 (M+1); Anal. Calcd for C, 65.25; H, 4.95; N, 14.73; Found: C, 65.58; H, 5.08; N, 14.44.

Cell lines and culture conditions. HepG-2 (liver), A549 (lung), MCF-7 (breast) and Hela (cervical) cancer cell lines were procured from ATCC (Manassas, VA, US). The HepG-2 cell line was cultured in media formulated by ATCC (Eagle's Minimum Essential Medium, Catalog No. 30-2003). A549, MCF-7 and Hela cells were grown in DMEM {Dulbecco's modified Eagle's medium (DMEM) containing 10% fetal bovine serum (FBS), 2 mmol/ liter glutamine, and 100 units/ml penicillin and streptomycin}. Rest Cal72 and SaOS-2 cell lines were obtained from Korean Cell Bank (Seoul, Korea) and was propagated in DMEM added with FBS (10%) and antibiotic-antimycotic (1%) solution. All cell lines were kept at 37°C in a humidified 95% air, 5% CO_2 atmosphere incubator designated as culture at a steady-state condition.[37-39]

Cytotoxicity assay. Briefly, a 100 µl cell suspension at a density of 4,000 cells each well was seeded in 96-well plate (Nunc™, Wiesbaden, Germany). After 24 hours recovery period, the cells were incubated in standard humid conditions and treated with synthesized compounds 5-16. The cells were treated with varying concentrations of compounds 5-16 and Doxorubicin (10 µM)

separately. Tested compounds 5-16 were dissolved in molecular grade DMSO, reaching a final DMSO concentration of 0.5%. After 24 hours, incubation with compounds 5-16 and Doxorubicin, 25 µl of PBS containing 2.5 mg/ml of MTT was added to each well. After 4 hours, the medium was discarded and 100 µl DMSO was added to dissolve the formazan crystals and then cells were incubated for 4 hours (37˚C and 5% CO_2). The light absorbance was measured at 590 nm by the Model 680 microplate-reader (Bio-Rad, Berkeley, CA, USA).[37-39]

Hoechst 33342 staining: The Cal72 cells were visualized for the apoptotic morphological changes in their nuclear chromatin by Hoechst 33342 staining by following our earlier reported methods.[37,39] The standard drug Doxorubicin was tested at 10 µM while, MCS-5 was tested by using 5 and 10 µM concentration.

Apoptosis assay by flow cytometry: Cal72 harvested cells were trypsinized (0.2 % EDTA-Trypsin) and then suspended in 4 ml fresh complete media and propagated in T25 flask and incubated overnight. Then, MCS-5 at 5 and 10 µM final concentrations was added and incubated for 24 hours. After 24 hours, PI/Annexin-V FITC double staining was carried out according to our standardized protocol.[39]

Early and Late apoptosis by PI/Annexin-V-FITC double staining. On the basis of morphological changes and pre and late apoptotic cells induced by MCS-5 in Cal72 cells were analyzed using PI/Annexin-V-FITC double staining assay. Contrast, Cal72 cells were seeded in four chambered culture slide (SPL, Life Sciences, Korea) followed by treatment with MCS-5 (5 µM/mL and 10 µM/ml) for 24 hours. After the incubation time, extract-untreated and treated Cal72 cells were harvested and washed with cold 1X PBS. Afterwards, 2 µl Annexin-V-FITC and 2 µl PI (50 µg/ml) were added to the suspension. The mixture was incubated for 30 min in the dark at room temperature. Stained cells were examined on slides via fluorescence microscopy (Olympus) using an excitation wavelength of 488 nm and a 515 nm filter in the detection pathway.

Cell cycle analysis. Cell cycle analysis was accomplished by using FACS according to our previously described process.[37] Cal72 cells were treated with MCS-5 at 5 µM and 10 µM

concentration, whereas 10 μM concentration of Doxorubicin was taken separately to compare the results.

Immunofluorescence staining: Cal72 cells were seeded in 4-well chambered slide with glass coverslips (SPL Life Sciences Co., Ltd., Korea). The cells were incubated with MCS-5 (5 and 10 μM) and Doxorubicin (10 μM) and non-treated cells incubated with DMEM high glucose medium for 24 hours. After the incubation time period, cells were washed carefully with 1X cold PBS and fixed with 4% paraformaldehyde for 15 minutes Then after, cells were permeabilized with 0.2% Triton X-100 for 10 min followed by washing with PBS and blocked with 1% bovine serum albumin (BSA) for 30 minutes Further, the cells were incubated with the primary antibodies (detailed in western blot analysis) and were detected using 1:200 rabbit IgG and mouse IgG. Afterward, the cells were incubated with Alexa Fluor 488, Alexa Fluor 647 and GFP conjugated (donkey anti-rabbit/anti-mouse) secondary antibodies for 1 hour at 25˚C in the dark. All of the antibodies except cytochrome-c and Apaf-1 (Cell Signaling) used were obtained from Santa Cruz Biotechnology, Inc. CA. Cells were then washed with cold PBS and were counterstained with 4',6-diamidino-2-phenylindole (DAPI, Invitrogen) for 5 minutes Once again cells were washed with cold 1X PBS and 1 ml mounting media was added and cells were observed under a fluorescence microscope (Olympus, Milan, Italy).[38]

Quantitative real-time polymerase chain reaction (qPCR): The relative cDNA synthesis was performed according to our formerly described laboratory protocol.[37-38] The cDNA was employed to qPCR for the quantification of the relative transcript levels of NF-κB (p65), Bcl-2, Bax, p53, cytochrome-c, Apaf-1, inflammatory cytokine IL-6 casp-3, and casp-9, using the specific primers (Table S1; supplementary information). β-actin opted as endogenous control.

Western blot analysis. Western blot analysis of protein of interest was carried out using procedure as described earlier.[37-38] Altogether, the antibodies excluding cytochrome-c/Apaf-1 (Cell Signaling) used were bought from Santa Cruz Biotechnology, USA. The PVDF membrane was incubated with the primary antibodies β-actin (1:1,000), anti-NF-κB (1:200), casp-3, casp-9, anti-human-IL-6, Bcl-2, Bax, anti-p53, cytochrome-c, Apaf-1 (mouse monoclonal IgG) were detected using 1:200 dilution. The proteins of interest were recognized by a greater chemiluminescence detection kit using LAS4000 machine (GE Healthcare, USA).

Determination of mitochondrial membrane potential (ΔΨm). Cal72 cells were originally seeded onto T_{25} flask and allowed to grow to 70 percent confluence. The cells were then exposed for 24 hours with the addition of MCS-5 (5 and 10 μM) and Doxorubicin (10 μM) to determine the state of mitochondrial membrane potential. The JC-1 dye was acquired from Sigma Aldrich and prepared in DMSO as a 5 mg/ml stock solution. Next day, to stain the cells, monolayers were rinsed with DMEM without phenol red (Sigma-Aldrich, USA). Cell monolayers were incubated with DMEM complete media and JC-1 5 (μg/ml) at 37˚C for 30 minutes. Further the cells were rinsed two times with DMEM and imaged using confocal fluorescence microscope set to excitation at 488 nm and detection at 510 nm to 525 nm (green) and 590 nm (red) channels using a dual band-pass filter. On the other hand, to determine **ΔΨm,** the cells were harvested and washed twice in cold PBS and then Centrifuge cells at 1200 rpm for 5 minutes at RT. The supernatent was removed and re-suspend cells in the 500 μl EDTA-1X PBS. Pipette and vortex to disrupt cell-to-cell clumping and the samples were analyzed by flow cytometry within one hour

Generation of intracellular ROS estimation by FACS. The Cal72 cells were seeded in T_{25} flask and incubated at 37ºC with 5% CO_2 until at least 70% confluent. Next day, cells were treated with varying concentrations, i.e. 5, 10 and 15 μM of MCS-5 and Doxorubicin, respectively. After 24 hours of treatment exposure, the cells were then washed with cold HEPES buffered salt solution to remove traces of the original medium. The cells were trypsinized, harvested and re-suspended in 2 μM (final concentration) 2′7′-dichlorofluorescein diacetate fluorescent dye (DCF-DA, Sigma Aldrich) and then incubated for 30 minutes in dark at room temperature. Obtained fluorescence intensity was quantified with the help of FACS (BD Biosciences, India) and fluorescence microscope. The FL1-H channel was used to calculate the mean DCF fluorescence intensity based on measurements of 10,000 cells. The M1 range was deliberated as each sub-population percentage of cells displaying enhanced DCF-DA fluorescence.

Cal72-induced xenograft nude mice model. Immunodeficient nude mice (SPF/VAF; 5 weeks old) were procured from KS HI-TEC, Inc Korea. The experimental processes were prior approved by the institutional review board of the Department of Animal Biotechnology, Jeju

National University, Jeju Special Self-Governing Province, Korea. The animals were housed by providing appropriate environmental and nutritional conditions. The mice (10, 11, and 12 week-age) were sacrificed by following the standard protocols of the Jeju National University. In order to design tumorigenesis and metastasis induction experiment, 24 nude mice were distributed into four groups. Group one as positive control (n = 6, treated with Doxorubicin 10 mg/kg/day). A second group used as test group low dose (n = 6, treated with MCS-5, 5 mg/kg/day). Another third group opted as a test group for high dose (n = 6, treated with MCS-5 10 mg/kg/day). The fourth group was inoculated non-treated tumor group as negative control (n = 6). To induce Cal72 mediated tumorgenesis, $1x10^6$ Cal72 cells/ml concentrations of cells into lower right/left flanks of nude mouse by micro-needle syringe (29 gauge x 1⁄2" 12.7 mm needle, Ultra-Thin Plus™ Korea). After generation of successful tumor model MCS-5 (5 and 10 mg/kg) and Doxorubicin (10 mg/kg) treatment were provided up to 45 days. Then the animals sacrificed and the tumors were removed from all animals and weight.

Optical probe guided molecular imaging to study tumor metastasis. *In-vivo* tumor localization was performed to study pre- and intraoperative tumor localization in the real-time resection by using 2-DG optical probe, according to our established method.[38] The metastatic potential of Cal72 was studied by injecting subcutaneously Cal72 cells in nude mice. To study the potential of MCS-5 (5 and 10 mg/kg) against metastasis was analyzed as compared to Doxorubicin (10 mg/kg). Spontaneous metastasis induced by Cal72 cells in nude mice and effect of MCS-5 to vanish/slow down metastasis were carefully analyzed.

Acknowledgements

The authors CB Mishra is thankful to the University Grants Commission (UGC) for the award of Dr. D.S. Kothari postdoctoral fellowship, S Kumari is thankful to UGC for financial support, M Tiwari is thankful to the University of Delhi for financial assistance. RJ Mongre and DK Jeong are thankful to Next Generation Bio Green 21 Program organization for providing financial support; grant number PJ01117401, Rural Development Administration, Republic of Korea.

University Science Instrumentation (USIC), University of Delhi is acknowledged for providing NMR and Mass spectral characterization of the synthesized compounds.

Financial Interests

The authors declare no conflict of interest.

Supporting Information

Supporting Information Available: This material is available free of charge via the Internet.

NMR spectra, HPLC chromatogram and primer table

References

(1) http://www.who.int/mediacentre/factsheets/fs297/en/index.html (Accessed: 1 April 2016).

(2) Baskar, R., Lee, K. A., Yeo, R., and Yeoh, K.W. (2012) Cancer and radiation therapy: current advances and future directions. *Int J Med Sci.* 9, 193-199.

(3) Vanneman, M., and Dranoff, G. (2012) Combining immunotherapy and targeted therapies in cancer treatment. *Nat Rev Cancer.* 12, 237-251.

(4) Baloch, S. K., Ling, L., Qiu, H., Ma, L., Lin, H., Huang, S., Qi, J., Wang, X., Lu, G., and Yang, Y. (2014) Synthesis and biological evaluation of novel shikonin ester derivatives as potential anti-cancer agents. *RSC Adv*. 4, 35588-35596.

(5) Bubert, C., Leese, M. P., Mahon, M. F., Ferrandis, E., Regis-Lydi, S., Kasprzyk, P. G., Newman, S. P., Ho, Y. T., Purohit, A., Reed, M. J., and Potter, B. V. L. (2007) 3,17-Disubstituted 2-Alkylestra-1,3,5(10)-trien-3-ol Derivatives: Synthesis, *In-vitro* and *In-vivo* Anticancer Activity. *J. Med. Chem*. 50, 4431-4443.

(6) Armitage, J. O., Mauch, P. M., Harris, N L., Bierman, P. (2001) Non-Hodgkin Lymphomas in *Cancer: Principles and Practice of Oncology*, (Devita, V. T., Hellman, S., and Rosenberg, S. A., Ed) 6th ed, pp 2256-2315 Lippincott Williams and Wilkins, Philadelphia.

(7) Rang, H. P., Dale, M. M., and Ritter, J. M. (2012) Anticancer drugs in *Textbook of Pharmacology*, (Rang, H.P., Dale, M. M., Ed) 7th ed, pp 673-687 Elsevier Churchill Livingstone, Edinburgh.

(8) Barot, K. P., Nikolova, S., Ivanov, I., and Ghate, M. D. (2013) Novel Anticancer Agents and Targets: Recent Advances and Future Perspectives. *Mini Rev Med Chem.* 13, 1239-1255.

(9) Remesh, A. (2012) Toxicities of anticancer drugs and its management. *Int J Basic Clin Pharmacol*. 1, 2-12.

(10) Kranz, D., and Dobbelstein, M. A. (2012) Killer promoting survival: p53 as a selective means to avoid side effects of chemotherapy. *Cell Cycle*. 11, 2053-2054.

(11) http://www.cancer.org/cancer/osteosarcoma/ Detailedguide/osteosarcoma-key-statistics.

(12) David, S.G., and Gorlick, R. (2010) Osteosarcoma: A Review of Diagnosis, Management, and Treatment Strategies. *Clin. Adv. Hematol. Oncol.* 10, 705-718.

(13) Lewis, V. O. (2007) What's new in musculoskeletal oncology. *J Bone Joint Surg Am.* 89, 1399-1407.

(14) Hayashi, K., Zhao, M., Yamauchi, K., Yamamoto, N., Tsuchiya, H., Tomita, K., Kishimoto, H., Bouvet, M., and Hoffman, R. M. (2009) Systemic targeting of primary bone tumor and lung

metastasis of high-grade osteosarcoma in nude mice with a tumor-selective strain of Salmonella typhimurium. *Cell cycle*. 15, 870-875.

(15) Hayashi, K., Zhao, M., Yamauchi, K., Yamamoto, N., Tsuchiya, H., Tomita, K., and Hoffman, R. M. (2009) Cancer metastasis directly eradicated by targeted therapy with a modified Salmonella typhimurium. *J Cell Biochem*. 106, 992-998.

(16) Kimura, H., Tome, Y., Momiyama, M., Hayashi, K., Tsuchiya, H., Bouvet, M., and Hoffman, R. M. (2012) Imaging the inhibition by anti-β1 integrin antibody of lung seeding osteosarcoma cells in live mice. *Int J Cancer*. 131, 2077-2033.

(17) Frantz, M. C., and Wipf, P. (2010) Mitochondria as a target in treatment. *Environ Mol Mutagen*. 51, 462-475.

(18) Ahn, C. S., and Metallo, C. M. (2015) Mitochondria as biosynthetic factories for cancer proliferation. *Cancer Metab.* 25, 1-10.

(19) Ralph, S. J., Low, P., Dong, L., Lawen, A., and Neuzil, J. (2006) Mitocans: mitochondrial targeted anti-cancer drugs as improved therapies and related patent documents. *Recent Pat Anti-Canc.* 1, 327-346.

(20) Indran, I. R., Tufo, G., Pervaiz, S. and Brenner, C. (2011) Recent advances in apoptosis, mitochondria and drug resistance in cancer cells. *Biochim Biophys Acta.* 1807, 735-745.

(21) Berube, G. (2016) An overview of molecular hybrids in drug discovery. *Expert Opin Drug Discov.* 11, 281-305.

(22) Dias, K. S. T., and Viegas, C. (2014) Multi-Target Directed Drugs: A Modern Approach for Design of New Drugs for the treatment of Alzheimer's disease. *Curr Neuropharmacol.* 12, 239-255.

(23) Kane, J. M., Dudley, M. W., Sorensen, S. M., and Miller, F. P. (1988) 2,4-Dihydro-3H-1,2,4-triazole-3-thiones as potential antidepressant agents. *J. Med. Chem.* 31, 1253-1258.

(24) Navidpour, L., Shafaroodi, H., Abdi, K., Amini, M., Ghahremani, M. H., Dehpour, A. R., and Shafiee, A. (2006) Design, synthesis, and biological evaluation of substituted 3-alkylthio-4, 5-diaryl-4H-1, 2, 4-triazoles as selective COX-2 inhibitors. *Bioorg. Med. Chem.* 14, 2507-2517.

(25) Guzeldemirci, N. U. and Kucukbasmaci, O. (2010) Synthesis and antimicrobial activity evaluation of new 1,2,4-triazoles and 1,3,4-thiadiazoles bearing imidazo[2,1-b]thiazole moiety. *Eur. J.Med. Chem.* 45, 63-68.

(26) Guniz Kucukguzel, S., and Cıkla-Suzgun, P. (2015) Recent advances bioactive 1,2,4-triazole-3-thiones. *Eur. J. Med. Chem.* 97, 830-870.

(27) Li, Z., Gu, Z., Yin, K., Zhang, R., Deng, Q., and Xiang, J. (2009) Synthesis of substituted phenyl-1,2,4-triazol-3-thione analogues with modified D-glucopyranosyl residues and their antiproliferative activities. *Eur. J Med. Chem.* 44, 4716-4720.

(28) Behari, J., Zeng, G., Otruba, W., Thompson, M., Muller, P., Micsenyi, A., Sekhon, S. S., Leoni, L., and Monga, S. P. S. (2007) R-Etodolac decreases beta-catenin levels along with survival and proliferation of hepatoma cells. *J. Hepatol.* 46, 849-857.

(29) Cheng, J., Imanishi, H., Liu, W., Nakamura, H., Morisaki, T., Higashino, K. and Hada, T. (2004) Involvement of cell cycle regulatory proteins and MAP kinase signaling pathway in

growth inhibition and cell cycle arrest by a selective cyclooxygenase 2 inhibitor, etodolac, in human hepatocellular carcinoma cell lines. *Cancer Sci.* 95, 666-673.

(30) Mavrova, A. T., Wesselinova, D., Tsenov, Y. A., and Denkova, P. (2009) Synthesis, cytotoxicity and effects of some 1,2,4-triazole and 1,3,4-thiadiazole derivatives on immunocompetent cells. *Eur. J. Med. Chem*. 44, 63-69.

(31) Singha, T., Singh, J., Naskar, A., Ghosh, T., Mondal, A., Kundu, M., Harwansh, R. K., and Maity, T. K. (2012) Synthesis and evaluation of antiproliferative activity of 1,2,4-triazole derivatives against EAC bearing mice model. *Ind. J. Pharm. Educ. Res*. 46, 346-351.

(32) Romagnoli, R., Baraldi, P. G., Cruz-Lopez, O., Cara, C. L., Carrion, M. D., Brancale, A., Hamel, E., Chen, L., Bortolozzi, R., Basso, G., and Viola G. (2010) Synthesis and Antitumor Activity of 1,5-Disubstituted 1,2,4-Triazoles as Cis-Restricted Combretastatin Analogues. *J. Med. Chem.* 53, 4248-4258.

(33) Zeng, S., Liu, W., Nie, F., Zhao, Q., Rong, J., Wang, J., Tao, L., Qi, Q., Lu, N., Li, Z., and Guo, Q. L. (2009) LYG-202, a new flavonoid with piperazine substitution, shows antitumor effects *in-vivo* and *in-vitro*. *Biochem Biophys Res Commun.* 385, 551-556.

(34) Shaquiquzzaman, M., Verma, G., Marella, A., Akhter, M., Akhtar, W., Khan, M. F., Tasneem, S. and Alam, M. M. (2015) Piperazine scaffold: A remarkable tool in generation of diverse pharmacological agents. *Eur. J. Med. Chem.* 102, 487-529.

(35) Sleijfer, S., Wiemer, E. and Verweij, J. (2008) Drug Insight: gastrointestinal stromal tumors (GIST)-the solid tumor model for cancer-specific treatment. *Oncology*. 5, 102-111.

(36) Zeng, S., Liu, W., Nie, F., Zhao, Q., Rong, J., Wang, J., Tao, L., Qi, Q., Lu, N., Li, Z., and Guo, Qi. (2009) LYG-202, a new flavonoid with a piperazine substitution, shows antitumor effects in vivo and in vitro. *Biochem. Biophys. Res. Commun*. 385, 551-556.

(37) Mongre, R. K., Sodhi, S. S., Ghosh, M., Kim, J. H., Kim, N., Park, Y. H., Kim, S. J., Heo, Y. J., Sharma, N., and Jeong, D. K. (2015) The novel inhibitor BRM270 down regulates tumorigenesis by suppression of NF-κB signaling cascade in MDR-induced stem like cancer-initiating cells. *Int J Oncol.* 46, 2573-2585.

(38) Mongre, R. K., Sodhi, S. S., Sharma, N., Ghosh, M., Kim, J. H., Kim, N., Park, Y. H., Shin, Y. G., Kim S. J, Jiao, Z. J., Huynh, D. L., and Jeong D. K. (2016) Epigenetic induction of epithelial to mesenchymal transition by LCN2 mediates metastasis and tumorigenesis, which is abrogated by NF-κB inhibitor BRM270 in a xenograft model of lung adenocarcinoma. *Int J Oncol.* 48, 84-98.

(39) Mishra, C. B., Mongre, R. K., Kumari, S., Jeong, D. K. and Tiwari, M. (2016) Synthesis, *in-vitro* and *in-vivo* anticancer activity of novel 1-(4-imino-1-substituted-1H-pyrazolo[3,4-d] pyrimidin-5(4H)-yl)urea derivatives. *RSC Adv.* 6, 24491-24500.

(40) Green, D. R., and Walczak, H. (2013) Apoptosis therapy: driving cancers down the road to ruin. *Nat Med*. 19, 131-133.

(41) Daniele, S. (2014) Apoptosis Therapy in Cancer: The First Single-molecule Co-activating p53 and the Translocator Protein in Glioblastoma. *Sci. Rep*. 4**,** 1-13.

(42) Senese, S., Lo, Y. C., Huang, D., Zangle, T. A., Gholkar, A. A., Robert, L., Homet, B., Ribas, A., Summers, M. K., Teitel, M. A., Damoiseaux, R., and Torres, J. Z. (2014) Chemical

dissection of the cell cycle: probes for cell biology and anti-cancer drug development. *Cell Death Dis.*5, 1-11.

(43) Cheng, T. (2004) Cell cycle inhibitors in normal and tumor stem cells. *Oncogene*. 23, 7256-7266.

(44) Yang, J., Liu, X., Bhalla, K., Kim, C. N., Ibrado, A. M., Cai, J., Peng, T., Jones, D. P., and Wang, X. (1997) Prevention of apoptosis by Bcl-2: release of cytochrome c from mitochondria blocked. *Science.* 275, 1129-1132.

(45) Tait, S. W. G., and Green, D. R. (2010) Mitochondria and cell death: outer membrane permeabilization and beyond. *Nat Rev Mol Cell Biol*. 11, 621-632.

(46) Fridman, J. S., and Lowe, S. W. (2003) Control of apoptosis by p53. *Oncogene.* 22, 9030-9040.

(47) Hoffman, B., and Liebermann D. A. (2008) Apoptotic signaling by c-MYC. *Oncogene.* 27, 6462-6472.

(48) Hajrezaie, M., Paydar, M. J., Looi, C. Y., Moghadamtousi, S. Z., Hassandarvish, P., Salga, M. S., Karimian, H., Shams, K., Zahedifard, M., Majid, N. A., Ali H. M., and Abdulla, M. A. (2015) Apoptotic effect of novel Schiff Based $CdCl_2$ ($C_{14}H_{21}N_3O_2$) complex is mediated via activation of the mitochondrial pathway in colon cancer cells. *Sci. Rep*. 5, 1-11.

(49) Karin, M., and Greten, F. R. (2005) NF-κB: linking inflammation and immunity to cancer development and progression. *Nat. Rev. Immunol.* 5, 749-759.

(50) Higuchi, M., Honda, T., Proske R. J., and Yeh, E. T. H. (1998) Regulation of reactive oxygen species-induced apoptosis and necrosis by caspase 3-like proteases. *Oncogene.* 17, 2753-2760.

(51) Liou, G., and Storz, P. (2010) Reactive oxygen species in cancer. *Free Radic Res.* 44, 479-496.

(52) Waterhouse, N. J., Goldstein, J. C., Ahsen, O. V., Schuler, M., Newmeyer, D. D., and Green, D. R. (2001) Cytochrome c maintains mitochondrial transmembrane potential and ATP generation after outer mitochondrial membrane permeabilization during the apoptotic process. *J Cell Biol.* 153, 319-328.

(53) Kim, W. H., Lee, J., Jung, D., and Williams, D. R. (2012) Visualizing Sweetness: Increasingly Diverse Applications for Fluorescent-Tagged Glucose Bioprobes and Their Recent Structural Modifications. *Sensors*. 12, 5005-5027.

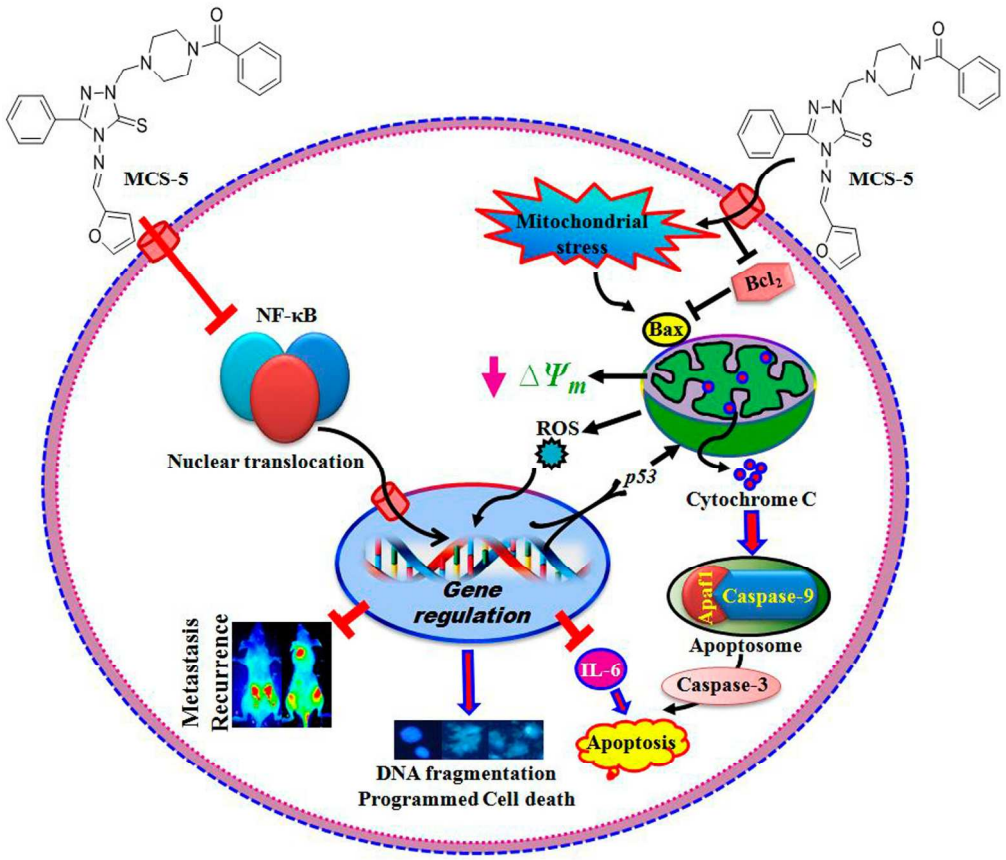

Graphical Abstract

200x176mm (300 x 300 DPI)

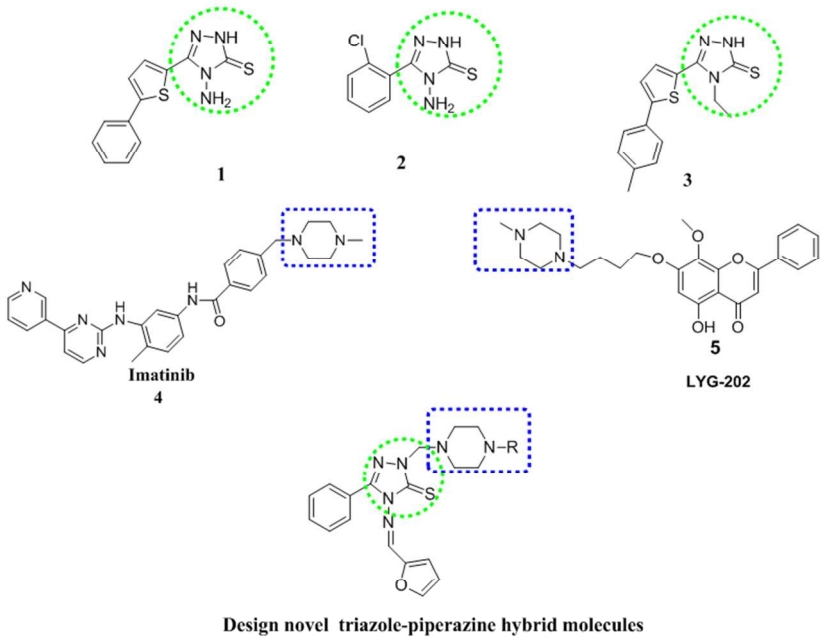

Figure 1. Potent anticancer agents in preclinical or clinical trial studies and designed triazole-piperazine hybrid molecules.

254x190mm (96 x 96 DPI)

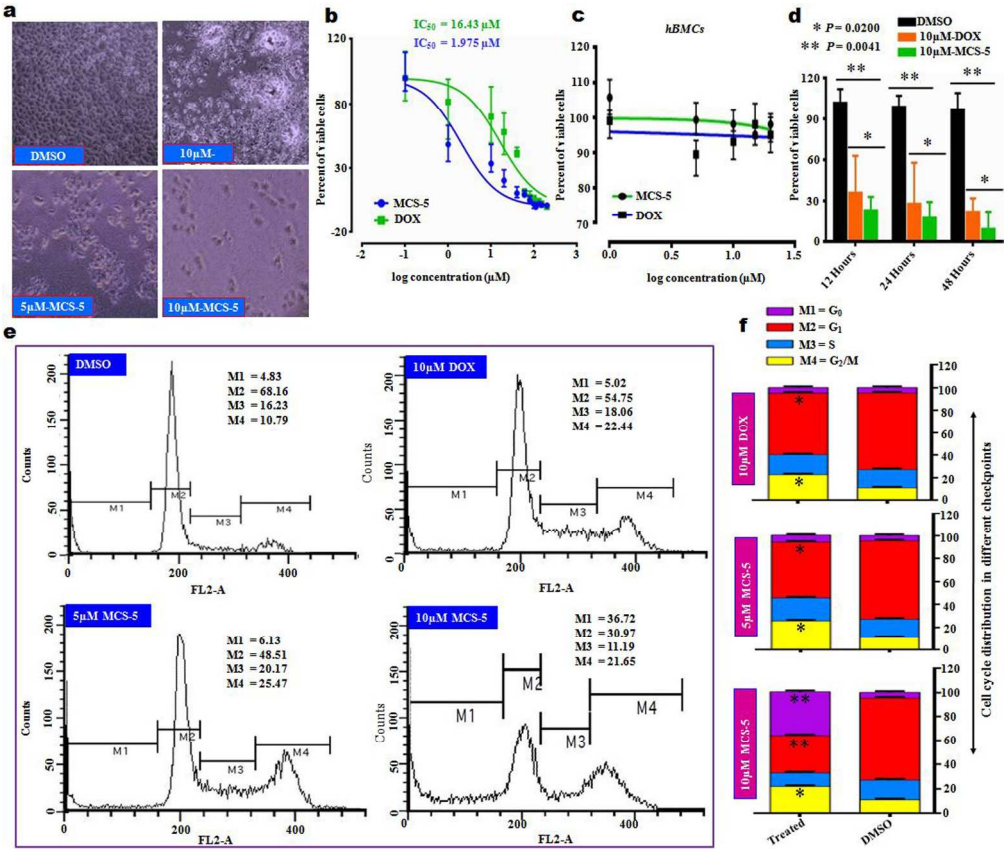

Figure 2. Cytotoxic effect of MCS-5 against Cal72 cells in dose and time dependent manner causes programmed cell death (a) Phase contrast micrographs showed cytotoxic effect exerted by MCS-5 (10 μM) and Doxorubicin (10 μM) against Cal72 cells after 24 hours exposure; Photographs were taken in a bright field microscope at 20x magnification. (b) Cal72 cells were treated with varying concentrations of MCS-5, Doxorubicin and the percentage viability as well as IC50 were determined by MTT assay at 24 hours. (c) Comparatively cytotoxicity effect of MCS-5 and Doxorubicin against normal cells hBMCs. (d) Time dependent cytotoxicity effect of MCS-5 against Cal72 cells up to 48 hours. (e) Cell cycle analysis of Cal72 cancer cells after being cultured with MCS-5 with respect to Doxorubicin for 24 hours showing an increase in G2/M phase cells (%).(f) Percent of cells in various checkpoints in the cell cycle distribution. The percentage of distributed cells in different cell cycle checkpoints are presented as mean (n = 3).* $p < 0.05$ versus the percentage of apoptotic cells of the control.

230x194mm (300 x 300 DPI)

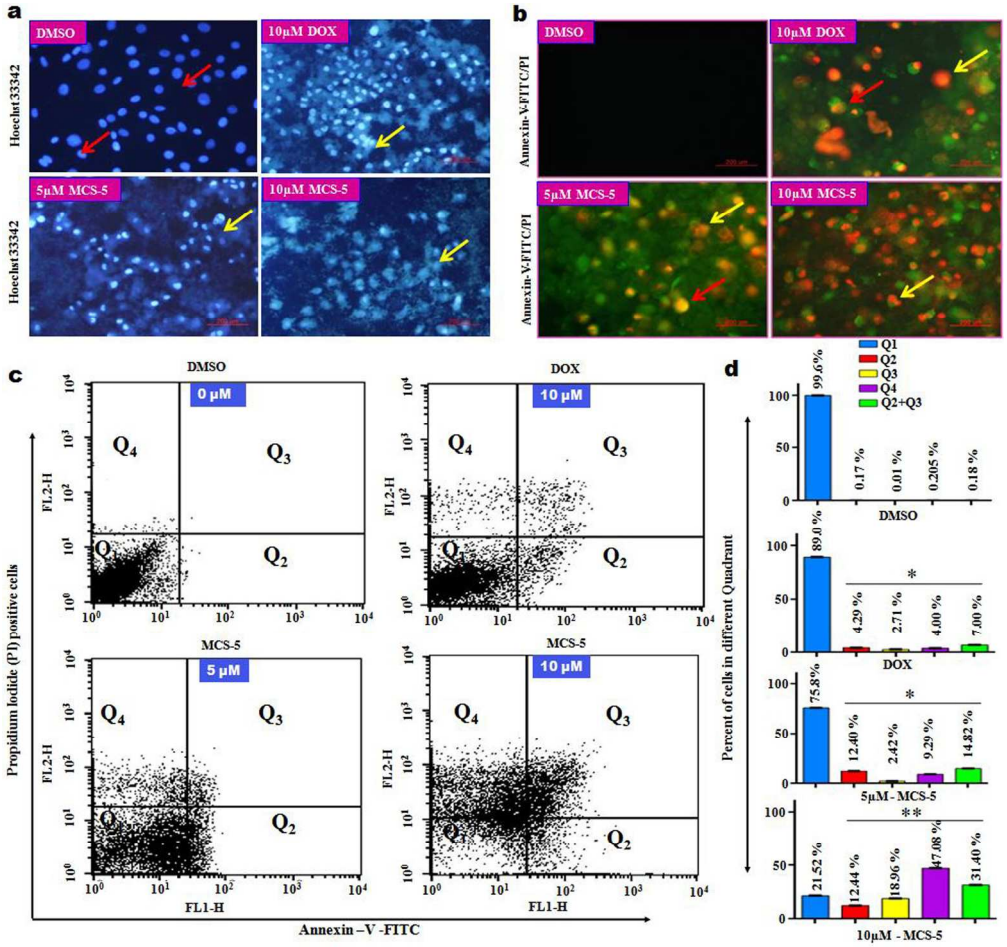

Figure 3. MCS-5 augmentes early and late apoptosis. (a) Effect of MCS-5 on Cal72 cells apoptosis. Fluorescent images of Hoechst 33342 staining displaying apoptosis associated morphological changes induced by MCS-5 and Doxorubicin after 24 hours treatment at 5μM and 10 μM concentrations. (b) Immunofluorescence apoptosis analysis of programmed cell death in Cal72 cancer cells based on the expression of early (Annexin-V: green) and late apoptotic cells red fluorescence positive cells (PI: red) after treatment with MCS-5 and Doxorubicin. Early features, including chromatin condensation and cell blabbing as well as DNA fragmentation were observed after 24 hours exposure with 5 μM and 10 μM MCS-5 and Doxorubicin respectively. The photos were taken using Olympus (Japan) flouroscnent microscope at 20X magnification. (c, d) Flow cytometric quadrant dot plot of apoptotic Cal72 cells after 24 hour treatment with MCS-5 and Doxorubicin. Apotosis of Cal72 cancer cells as identified by PI/ Annexin-V-FITC dual staining method. The percentage of viable cells, early apoptotic cells, late apoptotic cells, and necrotic cells are presented as mean (n = 3).* P < 0.05/** P < 0.001 versus the percentage of apoptotic cells of the control.

209x197mm (300 x 300 DPI)

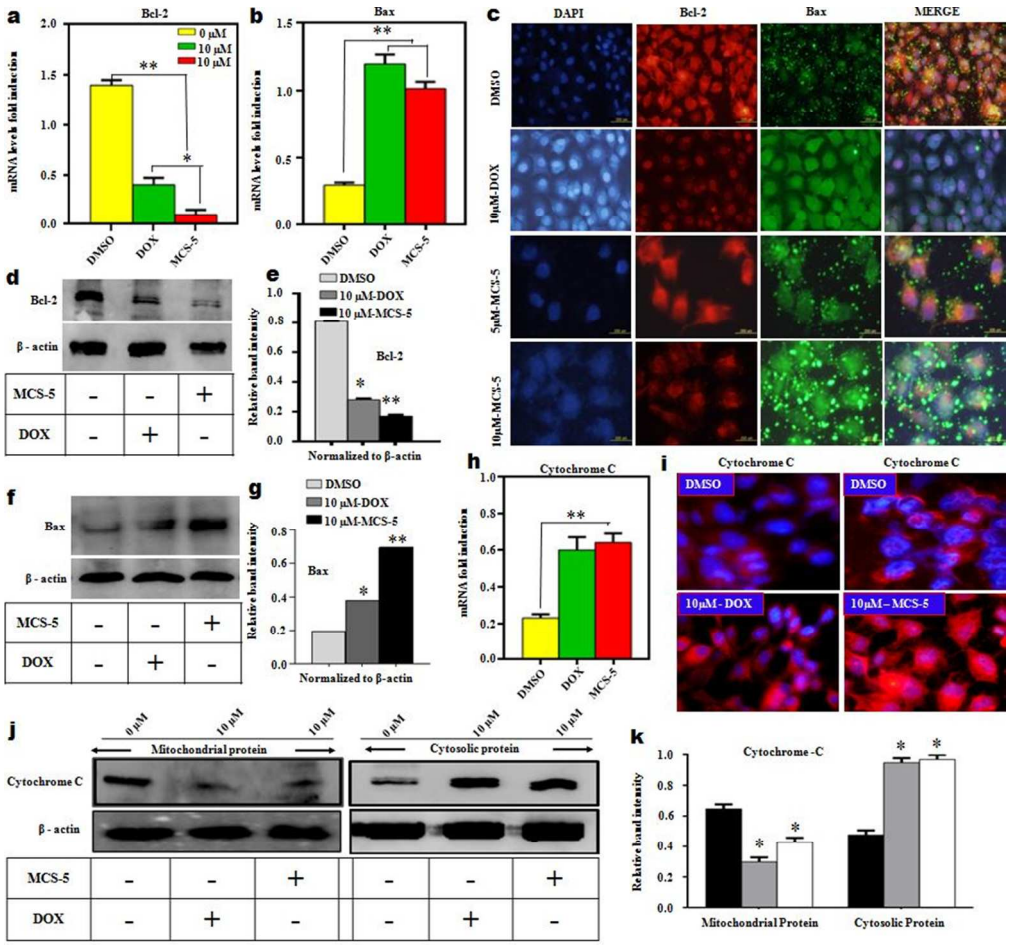

Figure 4. MCS-5 treatment downregulates Bcl-2 and activates mitochondrial intrinsic pathway. (a, b) Quantitative real time qRT-PCR was performed for the Bcl-2 and Bax. The data obtained from three independent cell samples are averaged with S.D. bars after normalization to β-actin mRNA signals. (c) Immunofluorescence evidence of expression of Bcl-2 and Bax showing significantly downregulated antiapoptotic Bcl-2 and upregulated Bax protein compared to control. Scale bar 20 μm. (d, e, f, g) Bax activation and Bcl-2 protein expression observed by western blot analysis, DMSO: untreated cell, Control: Doxorubicin treated cell, MCS-5 treated cells, with elative band intensity of caspase-3 by Image J software. (h) Quantitative real time qRT-PCR was performed for expression of Cytochrome-C. (i) Immunocytochemistry analysis of Cytochrome-C, fluorescence staining intensity observed in MCS-5 and Doxorubicin treated versus non-treated Cal72 cells. (j, k) The mitochondrial and cytosolic cytochrome c expression analyzed by western blot and Relative band intensity was measured using imageJ software. *P<0.05,**P<0.001 have been opted as significant differences.

243x227mm (96 x 96 DPI)

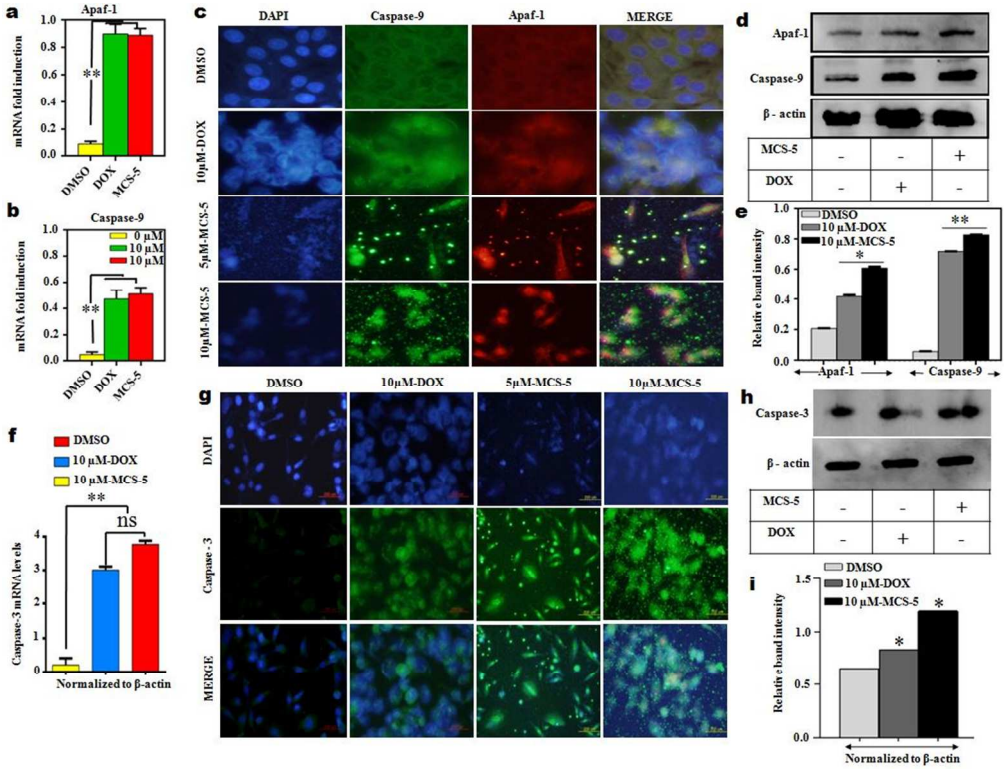

Figure 5. MCS-5 induces formation of apoptosome associated proteins complex that triggers activation of Casp-3 mediated intrinsic apoptosis pathway. (a, b) Quantitative real time qRT-PCR was performed for the Apaf-1 and Caspase-9. The data obtained from three independent cell samples are averaged with S.D. bars after normalization to β-actin mRNA signals. (c) Detection of apoptotic protein activation and formation of apoptosome by confocal microscopy. Cytochrome-C released from mitochondria and then triggers to increase activation and localization of Caspase-9 with Apaf-1 that significantly observed by immunocytochemistry compared to control and Doxorubicin treated cells. Scale bar, 20µm. (d, e) Cal72 cells were treated with 10µM MCS-5 and Doxorubicin for 24 hours then total protein harvested using RIPA cell lysis buffer. The investigation of the apoptosome forming associated protein levels were carried out by SDS-PAGE western blotting. (f) Quantitative real time qRT-PCR was performed to determine the mRNA levels of Caspase-3. The data obtained from three independent cell samples are averaged with S.D. bars after normalization to β-actin mRNA signals. (g) Cal72 cells were cultured with or without 5 and 10 µM MCS-5 or Doxorubicin for 24 hours for analysis of Caspase-3 activation. Confocal microscopy shows Caspase-3 expression (green fluoroscence) and DAPI staining (blue staining) in control as well as treated cells. (h, i) Immunoblot study conducted to analyse protein expression of Caspase-3 in MCS-5 and non-treated Cal72 cell protein lysate compared to Doxorubicin. *P<0.05,**P<0.001 have been opted as significant differences.

280x214mm (96 x 96 DPI)

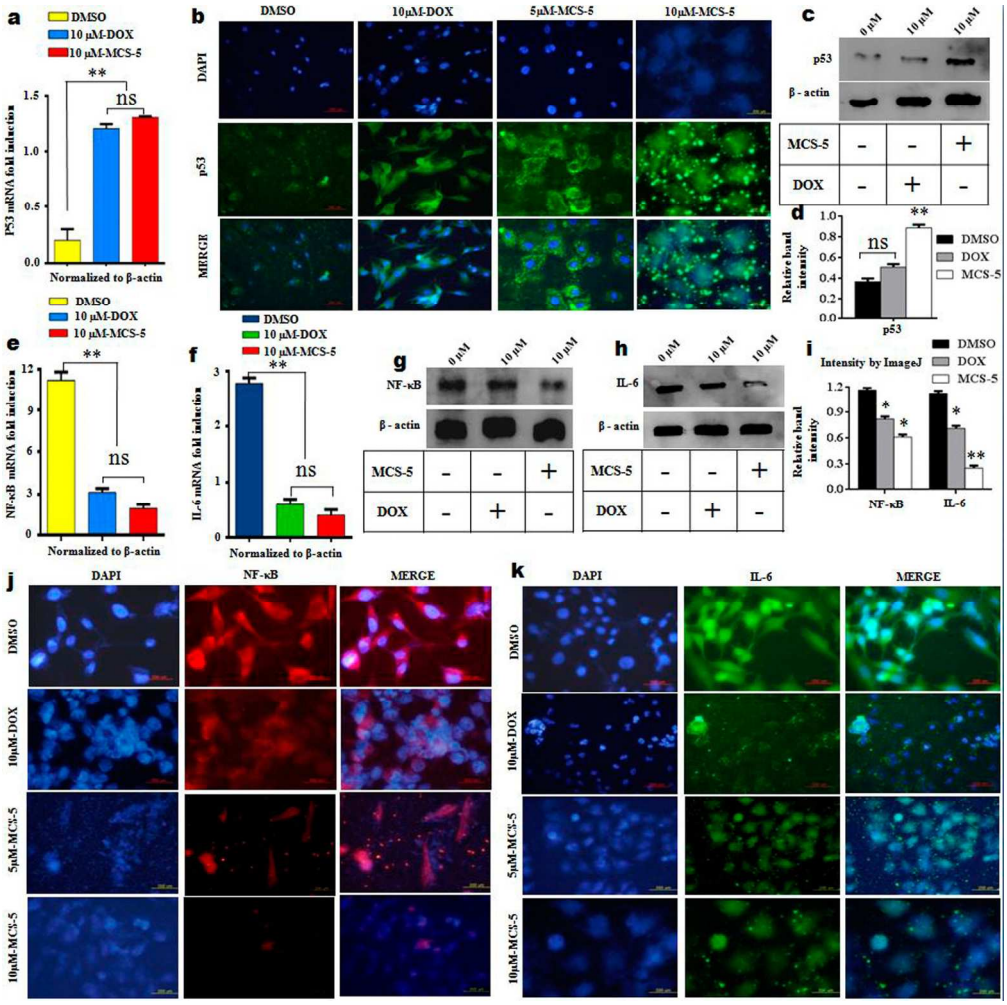

Figure 6. MCS-5 treatment induces p53 activation and NF-κB/IL-6 down-regulation which mediate apoptosis and programmed cell death. (a, e, f) Quantitative real time qRT-PCR was performed to determine the mRNA levels of p53, IL-6 and NF-κB. The data obtained from three independent cell samples are averaged with S.D. bars after normalization to β-actin mRNA signals. *P<0.05,**P<0.001 have been opted as significant differences. (b) Cal72 cells were cultured with or without 5 and 10 μM MCS-5 or Doxorubicin for 24 hours for immunocytochemistry analysis of p53 induction. (c, d, g, h, i) Immunoblot study conducted to analyze protein expression of p53, IL-6 and NF-κB in MCS-5 treated, and non-treated Cal72 cell protein lysate compared to Doxorubicin. (j, k) Cal72 cells were cultured with or without 5 and 10 μM MCS-5 or Doxorubicin for 24 hours for analysis of IL-6 suppression and NF-κB downregulation. Confocal microscopy shows IL-6 (green fluorescence) and NF-κB (red fluoroscence) expression and DAPI staining (blue staining) in control as well as treated cells. Scale bar, 10μm and 20μm

198x197mm (300 x 300 DPI)

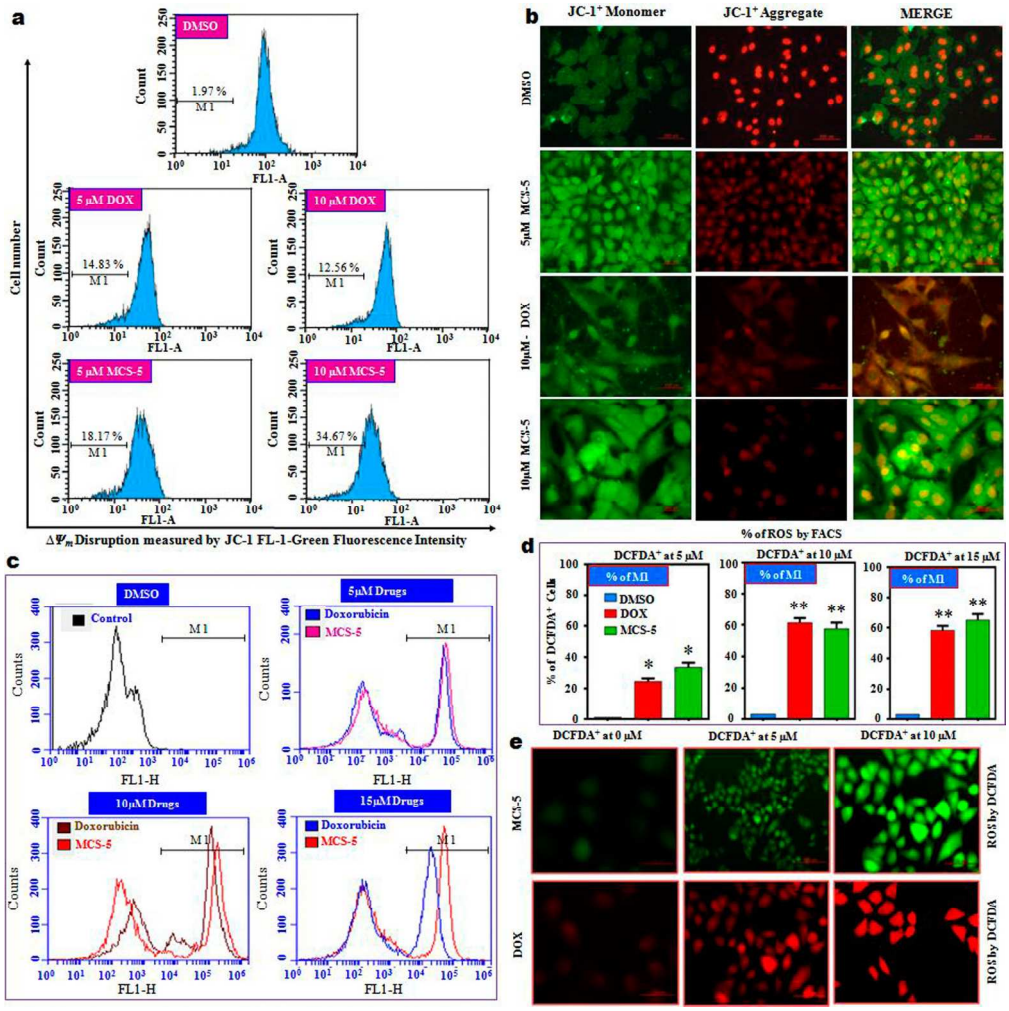

Figure 7. Antineoplastic efficacy of MCS-5 by collapsing the mitochondrial membrane potential (ΔΨm) and inducing ROS production Cal72 cancer cells. (a) Flow cytometric band shift plot of mitochondrial membrane potential in Cal72 cells, where Doxorubicin was used as a positive control. Cal72 cells were treated with 5 μM and 10 μM MCS-5 or 10 μM Doxorubicin for 24 hours and then ΔΨm was determined using JC-1 dye by flow cytometry. (b) 24 hours exposure with MCS-5 and Doxorubicin Cal72 cells then stained with JC-1 dye, the changes in MMP was measured using JC-1 fluorescence imaging. The JC-1 monomer was represented by green fluorescence, the JC-1 aggregate image was represented by red fluorescence, and the merged images were the combined of the green and red images. Control cells showed strong aggregated red fluorescence indicative of normal membrane potential. Scale bar = 100 μm. (c) Cells were treated with 5 μM and 10 μM MCS-5 or Doxorubicin for the indicated time periods, and the intracellular ROS (O2 and H2O2) levels were detected by flow cytometry using 2 μM H2-DCFDA as fluorescent probes as described in the Materials and methods section. (d) Percent bar graph of calculated M1 gated total cell count for DCFDA positive ROS producing Cal72 cells in MCS-5 and Doxorubicin respectively. (e) Intracellular ROS (O2 and H2O2) levels were detected by confocal microscopy study. Values are means ± S.E.M. for at least three independent experiments performed in triplicate (*P < 0.05 and **P < 0.01 compared with Doxorubicin alone).

197x198mm (300 x 300 DPI)

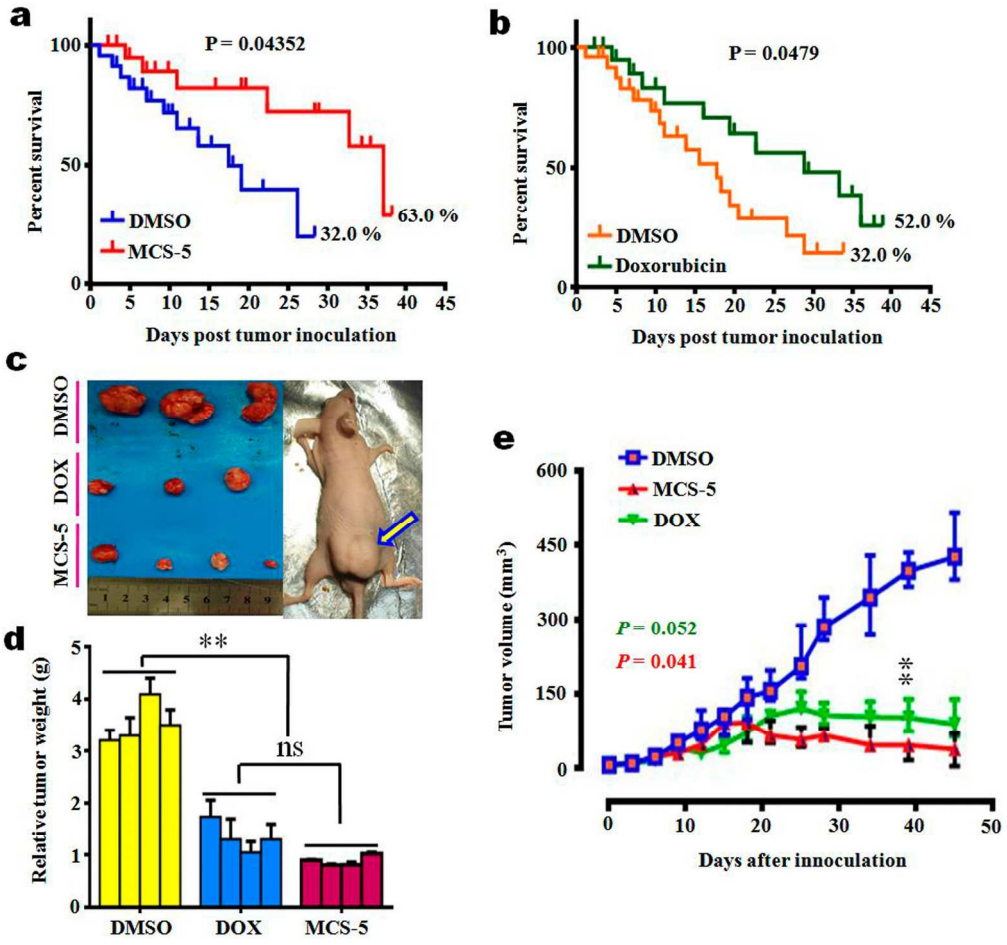

Figure 8. MCS-5 inhibits Cal72 induced tumor progression and mitigates metastasis in SPF/VAF immunodeficent nude mice. (a) Kaplan-Meier survival curves showing survival in Cal72 augmented osteosarcoma bearing nude mice which received MCS-5, showing decreased disease or metastasis free for untreated animals and MCS-5 (10mg/kg/day) treated animals. (b) Kaplan-Meier survival curves showing percentage survival in untreated and Doxorubicin (10mg/kg/day) treated animals (c) Extraction of tumor after 45 days, Control: represent untreated tumor, Doxorubicin: represent positive control (10mg/kg/day) treated tumor and MCS-5: represent MCS-5 (10mg/kg/day) treated tumor for 45 days. (d) Relative tumor weight in untreated animals, Doxorubicin (10mg/kg/day) treated animals and MCS-5 (5mg/kg and 10 mg/kg/day) treated animals (e) Tumor volume in untreated animals, Doxorubicin (10mg/kg/day) treated animals and MCS-5 (10mg/kg/day) treated animals. Data represent mean ± std err, *P<0.05, **P<0.001 determined by 2-way ANOVA followed by Tukey's comparison test.

203x190mm (300 x 300 DPI)

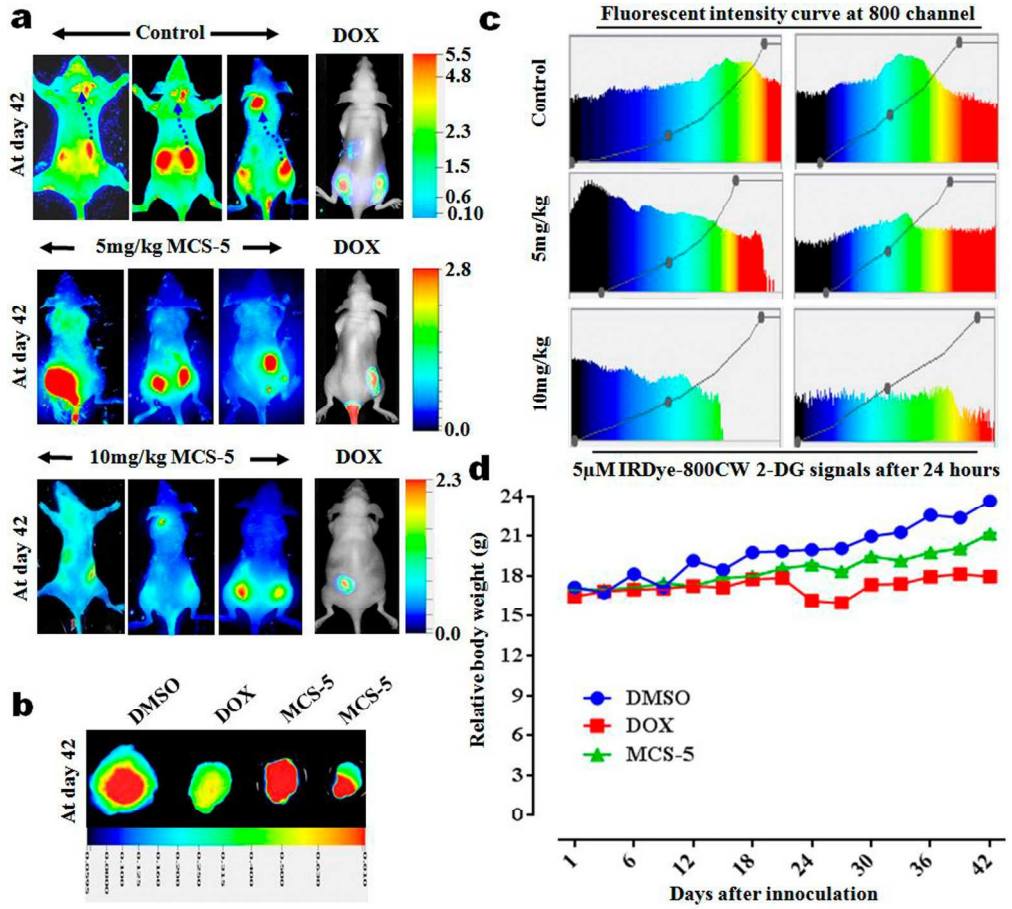

Figure 9. MCS-5 reduces metastatic dissemination and mitigates tumor progression in IRDye® -2DG guided molecular imaging xenograft model. (a) LI-COR Pearl image of untreated mice (control), Doxorubicin (10mg/kg) treated mice and MCS-5 (5mg/kg and 10 mg/kg) treated mice. (b) IRDye® near-infrared optical probe 2DG guided untreated tumor (control), Doxorubicin (10mg/kg) treated tumor and MCS-5(5mg/kg and 10 mg/kg) treated tumor. (c) IR Dye-800 CW-2DG signal observed after 24 hour in MCS-5 (5mg/kg and 10 mg/kg) treated animals as compared to control animals. Lower florescence intensity was observed in MCS-5 treated group as compare to control. (d) Relative body weight curve of mice in the same group. Data represent mean ± std err, *P<0.05, **P<0.001 determined by 2-way ANOVA followed by Tukey's comparison test.

203x183mm (300 x 300 DPI)